Science of the Total Environment 639 (2018) 961–976

Contents lists available at ScienceDirect

Science of the Total Environment

journal homepage: www.elsevier.com/locate/scitotenv

Future climate and cryosphere impacts on the hydrology of a scarcely gauged catchment on the Jhelum river basin, Northern Pakistan

Muhammad Azmat [a,b,*], Muhammad Uzair Qamar [c], Christian Huggel [a], Ejaz Hussain [b]

[a] Department of Geography, University of Zurich, 8057 Zurich, Switzerland
[b] Institute of Geographical Information Systems (IGIS), National University of Sciences and Technology (NUST), Islamabad, Pakistan
[c] Department of Irrigation and Drainage, University of Agriculture, Faisalabad, Pakistan

HIGHLIGHTS

- The high-altitude scarcely-gauged Himalayan catchments are the hotspot to climate change.
- Over high-altitude basins, better suited GCMs, bias corrections and hydrological models are of the high importance.
- Positive precipitation and temperature trends over the basin alters the hydrological regime.
- ET, soil water storage, snow- and rainfall-runoff likely to increase under future scenarios.
- Temperature rise is accelerating the early snowmelt process, resulting alters the hydrological regime.

GRAPHICAL ABSTRACT

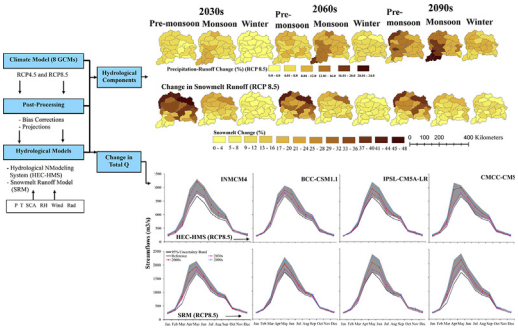

ARTICLE INFO

Article history:
Received 31 October 2017
Received in revised form 16 May 2018
Accepted 17 May 2018
Available online 26 May 2018

Keywords:
Climate models
Bias corrections
Hydrological modelling
Precipitation- and snowmelt-runoff
Climate change

ABSTRACT

Streamflow projections are fundamental sources for future water resources strategic planning and management, particularly in high-altitude scarcely-gauged basins located in high mountain Asia. Therefore, quantification of the climate change impacts on major hydrological components (evapotranspiration, soil water storage, snowmelt-runoff, rainfall-runoff and streamflow) is of high importance and remains a challenge. For this purpose, we analysed general circulation models (GCMs) using a multiple bias correction approach and two different hydrological models i.e. the Hydrological Modelling System (HEC-HMS) and the Snowmelt Runoff Model (SRM), to examine the impact of climate change on the hydrological behaviour of the Jhelum River basin. Based on scrutiny, climate projections using four best fit CMIP5 GCMs (i.e. BCC-CSM1.1, INMCM4, IPSL-CM5A-LR and CMCC-CMS) were chosen by evaluating linear scaling, local intensity scaling (LOCI) and distribution mapping (DM) approaches at twenty climate stations. Subsequently, after calibration and validation of HEC-HMS and SRM at five streamflow gauging stations, the bias corrected projected climate data was integrated with HEC-HMS and SRM to simulate projected streamflow. Results demonstrate that the DM approach fitted the projections best. The climate projections exhibited maximum intra-annual rises in precipitation by 183.2 mm (12.74%) during the monsoon for RCP4.5 and a rise in T_{min} (T_{max}) by 4.77 °C (4.42 °C) during pre-monsoon, for RCP8.5 during 2090s. The precipitation and temperature rise is expected to expedite and increase snowmelt-runoff up to 48% and evapotranspiration and soil water storage up to 45%. The projections exhibited significant increases in streamflows by 330 m^3/s (22.6%) for HEC-HMS and 449 m^3/s (30.7%) for SRM during the pre-monfaf0000soon season by the 2090s under RCP8.5. Overall, our results reveal that the pre-monsoon season is potentially utmost affected

* Corresponding author at: Department of Geography, University of Zurich, 8057 Zurich, Switzerland.
E-mail addresses: muhammad.azmat@geo.uzh.ch (M. Azmat), muhammad.uzair@uaf.edu.pk (M.U. Qamar), christian.huggel@geo.uzh.ch (C. Huggel), ejaz@igis.nust.edu.pk (E. Hussain).

https://doi.org/10.1016/j.scitotenv.2018.05.206
0048-9697/© 2018 Elsevier B.V. All rights reserved.

under scenario-periods, and consequently, which has the potential to alter the precipitation and flow regime of the Jhelum River basin due to significant early snow- and glacier-melt.

© 2018 Elsevier B.V. All rights reserved.

1. Introduction

Streamflow predictions for a changing climate are tremendously important for better water resources strategic planning and management, including floods, droughts and sustainable agriculture, particularly for the regions which significantly rely on water originating from snow- and glacier-fed catchments. However, such climate change investigations are largely associated with climate projections derived from general circulation models (GCMs) (Lutz et al., 2016b). The uncertainties in projected climate data restrain the robustness of investigations, consequently leading to less confident conclusions, particularly in high-altitude regions with limited data are executed (Forsythe et al., 2014). The potential implications of changes in climate on hydrological regime of such regions are of high importance and remain a challenge. However, the selection of an appropriate hydrological model can be difficult for high-altitude regions with rainfall and snow- and glacier-melt contribution to runoff. The majority of the hydrological models performed less efficiently in high-altitude regions due to scarce climate data issues and structural design algorithms (Martinec et al., 2008). Generally, the hydrological models are categorized into snowmelt- and rainfall-runoff algorithms based applications depending on characteristics (rainfall- or snowmelt-runoff dominant). However, their application with sufficient accuracy in such regions and the integration of other components of climate projections (models or methods) remains a challenge. The biases in projected climate data play a significant role for the inaccuracy of hydrological projections. These biases could further question hydrological predictions due to the selection of inappropriate hydrological models for a particular catchment, and consequently, streamflow simulation and forecasting for a changing climate is rather challenging (Jiang et al., 2015). Thereby, the selection of an appropriate hydrological model, GCMs and bias correction techniques are tremendously important for the streamflow predictions to changing climate in catchment having both rainfall- and snowmelt-runoff sources, particularly with limited data. Limitations in in-situ observations along with the influence of different sources of water are well-known for the Hindukush-Karakoram and Himalayas (H-K) where snow and glacier contribute during the pre-monsoon and monsoon, while precipitation contributes primarily during monsoon season (Bolch et al., 2012). This region is influenced by a two-fold precipitation pattern such as the monsoon and westerlies circulations (Azmat et al., 2017a). The westerlies are responsible for nourishing seasonal and perennial snow and glacier of the northwest regions (Karakoram) by over two thirds, while strong monsoon contributes ≈80% precipitation over the southeast part (Himalayas) (Dahri et al., 2016). Recently, the Himalayan regions are considered as one of the hotspot to climate change which could influence millions of people by changing the hydrological regimes of the river basins (Bajracharya et al., 2018; Lutz et al., 2016a). These climate changes may be attributed to the diverse climate and topographic variations, therefore, the importance of such changes on hydrological behaviour of the region is of high importance to investigate (Bajracharya et al., 2018). Several researchers have attempted to investigate the behaviour of climate change on the hydrological regimes of snow- and glacier-fed catchments with the integration of projected climate variables derived from GCMs or RCMs (Regional Climate Models) and hydrological models, both worldwide, and specifically in the Himalayan region, (Bajracharya et al., 2018; Beniston and Stoffel, 2016; Lutz et al., 2014; Shrestha et al., 2017).

Lutz et al. (2014) and (2016a) applied a Spatial Processes in Hydrology (SPHY) model for the investigation of climate change implications on future water availability in different large scale high-altitude mountainous catchments (e.g. Indus, Ganges, Brahmaputra, Salween and Mekong) located in South Asia. Bajracharya et al. (2018) utilized scrutinized GCMs projected climate data at 10 km resolution developed by Lutz et al. (2016a) for the Indus, Ganges and Brahmaputra (IGB) basins with integration of the Soil and Water Assessment Tool (SWAT) model and provided estimates of water balance components to a changing climate in Kaligandaki Basin, Nepal.

Aforementioned and most of the previous studies focused on basins with comprehensive data over the catchments or low altitude regions with marginal snow- and glacier-melt contribution without considering suitability of hydrological models according to catchment characteristics. In the Jhelum River basin, to the best of our knowledge, no study so far has been carried out to quantify the water balance components under various climate change scenarios. This study is an attempt to examine the efficiency of different GCMs, bias correction techniques and hydrological models in the high-altitude snow- and glacier-fed scarcely-gauged Jhelum River basin located in western Himalayas. The specific objective of this study is to quantify the seasonal change on climate variables (precipitation and temperature) and on major hydrological components such as evapotranspiration, soil water storage, rainfall-, snowmelt-runoff and finally streamflows to potential climate change scenarios in Jhelum River basin. For this purpose, we utilized four most suitable GCMs out of eight (8), three bias correction techniques and two widely used hydrological models based on different algorithms (HEC-HMS; a rainfall runoff model and SRM; a snowmelt runoff model).

2. Study area

The Jhelum River basin is located in the west of the Himalayan range and is one of the most important sub-basins of Upper Indus Basin (UIB), therefore, the overall climate of the Jhelum River basin is dominated by two precipitation types, namely the Indian monsoon (during summer), and the winter precipitation from west (westerlies circulations) (Azmat et al., 2017a). The South Asian region including UIB and Himalayas is reported as a "Hotspot" to changes in climate according to several studies (Bajracharya et al., 2018; Lutz et al., 2014; Lutz et al., 2016a), and these changes in climate could significantly alter the water resources system due to significant contributions from snow and glaciers. Therefore, being one of the important sub-catchment of the UIB, the Jhelum River basin was selected in this study.

The Jhelum River with 33,867 km^2 of drainage area, is dammed by the Mangla reservoir which is Pakistan's second and world's seventh largest storage reservoir with 7.29 km^3 of gross storage capacity. The stored water in the reservoir is used to irrigate 6 million ha of agricultural area (Archer and Fowler, 2008). The selected study basin extends over the high mountains of the Western Himalayas and drains the southern slopes of the Himalayan range with approximately 14.98% area situated above 4000 m a.s.l. (Table S1 and Fig. 1). Administratively, Jhelum River is a trans-boundary catchment with approximately 56% (18,965 km^2) lying in India and 46% (14,902 km^2) in Pakistan. The climatic and hydrological behaviour of the Jhelum River basin is peculiar due to trans-boundary related scarcely-gauged issues and strongly influenced by twofold climate patterns (monsoon and westerlies

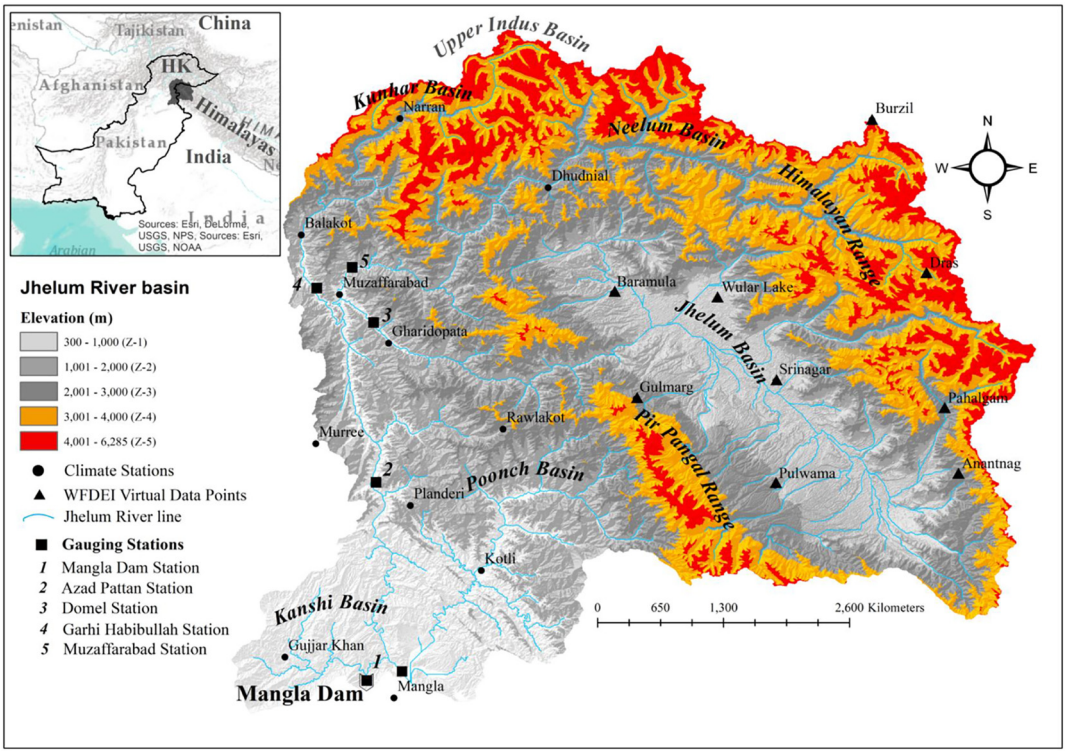

Fig. 1. Geographical location of Pakistan and the Jhelum River basin (study Area) including streamflow gauges, installed climate stations and virtual points of WFDEI data over un-gauged part of the basin.

circulation) in contrast to sub-catchments of UIB such as Astore, Hunza and Gilgit (which are influenced by westerlies circulation) and Chanab River basin (influenced by monsoon only). Additionally, this catchment receives major runoff contributions from snow- and glacier-melt during early summer (April to mid-June) which accumulates during the winter season by the influence of the westerlies circulation pattern, while monsoon precipitation contributes significantly during the summer season (end of June to August) (Fig. S1 and S2) (Lutz et al., 2016a). The above statement is confirmed by the fact that during the winter months (October to March), approximately 65% of the catchment (basin-wide) is covered by snow, which declines to about 3% by the end of summer (August) (Table S1). Further to this, almost 38% of mean annual rainfall occurs during winter season while the remaining 62% occurs during the summer season. Some key characteristics of the climate stations and data points for the part of the basin without any river runoff observations and altitude zones of the Jhelum River basin are given in Table S1 and shown Fig. 1.

3. Datasets

The recorded daily inflows of the Jhelum River at Mangla dam, Azad Pattan, Muzaffarabad, Garhi Habibullah and Domel gauging stations were obtained from the Surface Water Hydrology Project of the Water and Power Development Authority (SWHP-WAPDA) and Directorate of Mangla Dam (DMD) for the years 1995–2013 (see Fig. 1 and Table S1). Moving upstream in the Jhelum River basin, the snow cover area (SCA) for the respective gauging stations increases (summer to winter) over Mangla, Azad Pattan, Muzaffarabad, Garhi Habibullah and Domel basins with a range between 5 and 68%, 13–79%, 9–71%, 16–82% and 3–65%, respectively, estimated in this study. The daily climate data for precipitation, T_{min} (minimum temperature) and T_{max} (maximum temperature), of ten (10) climate stations inside the catchment located in Pakistan, were acquired from WAPDA and Pakistan Meteorological Department (PMD). Since, the Jhelum River is a trans-boundary river catchment, therefore, the daily bias corrected precipitation and temperature data (1979–2012) offered by the WATCH Forcing Data-ERA Interim (WFDEI) was downloaded (ftp://ftp.iiasa.ac.at/WATCH_Forcing_Data/WFDEI/) and extracted at nine virtual data points for the un-gauged part of the catchment located in India (Weedon et al., 2014). The integrity and application of this dataset has already been evaluated by several researchers in the Indus Basin (Dahri et al., 2016; Lutz et al., 2016b). Additionally, in order to force HEC-HMS to incorporate evapotranspiration, the short-wave and long-wave solar radiation (W/m^2), wind speed (m/s), air pressure (Pa), specific humidity (kg/kg) and sunshine hour data were obtained from Global Land Data Assimilation System (GLDAS). GLDAS provides a comprehensive integrated satellite and ground data to generate near real-time land surface circumstances (Rodell et al., 2004). Liaqat et al. (2015), have utilized GLDAS data products for land surface modelling in scarcely gauged regions.

In this study, the snow cover area (SCA) was extracted by using Moderate Resolution Imaging Spectroradiometer (MODIS) data utilized as an input of SRM, for the Jhelum River basin. Approximately, 638 processed MODIS aqua SCA product available at 8-day interval (MOD10A2) and terra available at daily time interval (MYD10A2) were downloaded from the NSIDC database (http://nsidc.org/data/search/) for the period between March 2000 to December 2014.

To simulate future hydrological conditions, the representative concentration pathways (RCPs) were utilized in this study available under the CMIP5 repository released during March 2013 (Taylor et al., 2012). We select eight (8) CMIP5 GCMs already screened by Lutz et al. (2016b) for the Upper Indus basin by using the "envelop based technique" to scrutinize the models for six subdomains (e.g. Lower Indus, Upper Indus, Lower Brahmaputtra, Upper Brahmaputtra, Upper Ganges and Lower Ganges). It is worth mentioning that the GCMs ranking in aforementioned study was assigned by considering skill score at aggregate level. However, we only select top ranked models for our area of interest (Upper Indus Basin). Table S2 depicts the detail of eight CMIP5 climate models used in this study.

4. Methods

4.1. Experimental design

We combined eight climate models, three bias correction techniques (linear scaling, local intensity scaling (LOCI), distribution mapping) and two different hydrological models (HEC-HMS and SRM) (see Fig. 2). We calibrated and validated both hydrological models on five gauging stations (Mangla, Azad Pattan, Domel, Neelum and Garhi Habibullah). While, the projected changes in streamflow was investigated at Mangla dam station by dividing each future scenario into further three sub-scenarios each comprised of 10 years (e.g. 2030s i.e. 2011–2020, 2021–2030, 2031–2040 and so on for 2060s and 2090s) to minimize expected uncertainties during hydrological modelling. In total 1152 hydrological projections were produced and examined. Overall, the proposed factorial design caters the possible risk regarding sample artefacts by examining numerous possible simulation combinations (see Fig. 2 and Table S3).

4.2. Evaluation of CMIP5 climate models and climate projections

In many cases, climate models provide substantial misrepresentation of the observed climate data, forcing correction measures (Teutschbein and Seibert, 2010; Teutschbein and Seibert, 2012). For this purpose, we employed three correction methods e.g. linear scaling, local intensity scaling (LOCI) and distribution mapping (DM). By considering efficiencies of bias correction approaches discussed by Teutschbein and Seibert (2012), linear scaling was adopted only for temperature and LOCI for precipitation, while, DM was used for both climate variables. The bias correction methods were applied by taking into account, GCM-simulations for control- (1976–2005) and scenario-periods [2030s (2011–2040), 2060s (2041–2070) and 2090s (2071–2100)] and observed control-period spanning 1976–2005. The detailed description for the applications and results of bias correction techniques used in this study is provided in the supplement material (see Figs. S4, S5 and S6). In order to evaluate CMIP5 model runs (GCMs) before and after bias correction, seven different statistical indices (i.e. mean (mm/d), standard deviation (mm/d), percentile (95%), 5-days maximum rainfall (mm), percent (%) wet days (wet threshold is equal to 1 mm), maximum dry spell length (days) and maximum wet spell length (days)) were used to demonstrate uncertainties in GCM-simulations in comparison with observed precipitation for different seasons [winter (Oct–March), pre-monsoon (April–June) and monsoon (July–Sep)] of control period (1976–2005), as provided in Table S4 and S5. The ranking were assigned to CMIP5 models by computing differences (biases) between quantified indices of model runs and observed precipitation which further analysed by taking mean value of all stations (basin-wide) against each model run, as provided in Table S5. While, in case of T_{min} and T_{max}, four established statistical indices (i.e. errors between observed data and model runs standard deviation (E_SD (°C)), errors between observed data mean and model runs mean (E_μ (°C)), root mean square error (RMSE) and correlation coefficient (R)) were computed before and after bias correction for each station against each model run, as provided in Table S6a. Subsequently, similar to precipitation, the mean of the indices for all climate stations (basin-wide) against the mean of each model run was compared to assign a ranking (Table S6).

4.3. Hydrological models

As discussed in Section 2, in the Jhelum River basin, the westerlies circulation is primarily responsible for snow accumulation while the summer season is mostly dominated by monsoon precipitation. Additionally, due to the scarcely-gauged and high-altitude characteristics of the catchment we decided to examine HEC-HMS and SRM hydrological models. Martinec et al. (2008), suggested that the majority of rainfall-runoff hydrological models perform less efficiently in high-altitude regions due to precipitation gauging errors and dominancy of snowmelt runoff. As shown previously, SRM performed better in such regions because of less sensitivity to precipitation resulting in less precipitation errors (Tahir et al., 2011). However, SRM is limited to provide only streamflows as output whereas HEC-HMS provides all major hydrological components (e.g. evapotranspiration-ET, soil water storage (SW), rainfall- and snowmelt-runoff etc.). Therefore, it is important to test hydrological models based on different algorithms (snowmelt- or rainfall-runoff) with data input and output limitations in catchments where precipitation and snow (hybrid) are equally important for runoff generation. We therefore applied these two widely used hydrological models; SRM, a standard snowmelt runoff model, uses remotely sensed cryosphere data as an input, and HEC-HMS, a standard rainfall runoff model with snowmelt runoff module, uses observed data to generate snow accumulation and melt, to analyse the suitability of the models in a high-altitude, scarcely-gauged catchment under control (reference) and climatic change scenario-periods (2030s, 2060s and 2090s). In this study, the change in hydrological components such as ET, SW, rainfall- and snowmelt-runoff contribution in response to a changing climate was computed by using HEC-HMS only, while the rainfall and snowmelt contribution using SRM model was estimated by adopting the

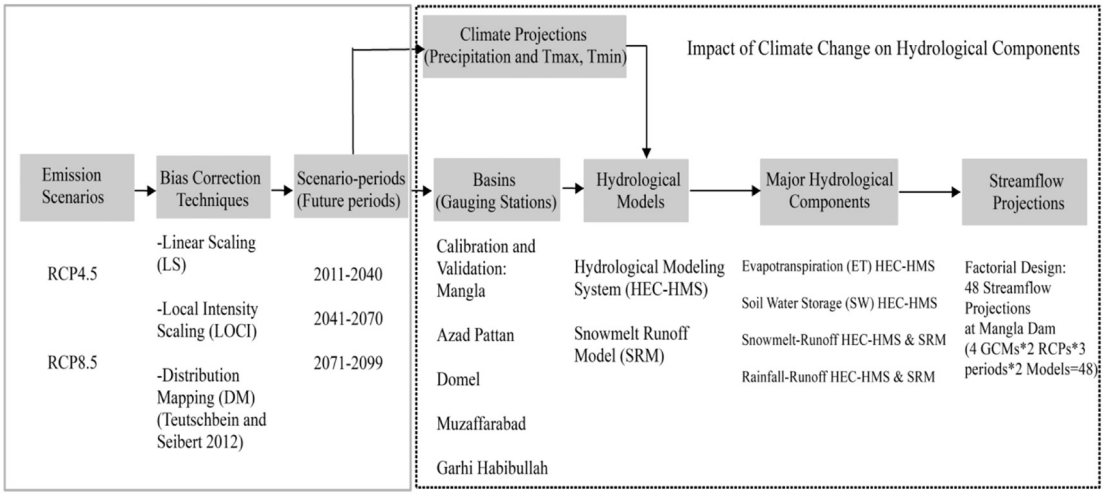

Fig. 2. Methodology flow chart adopted in this study, the boxes show major steps/elements required for streamflow projections. For each step multiple approaches were adopted, as listed below the box. Total GCMs were used to scrutinize four most suitable, for streamflow projections in Jhelum River basin.

methodology by Zhang et al. (2014). We applied both model using their most efficient methodologies (e.g. SRM: zone-wise and HEC-HMS: semi-distribution with extensive combination of methods for loss, transfer, ET and snowmelt), as discussed in the next section. Several researchers have successfully applied both models in rain-fed and snow and glacier dominant basins (Azmat et al., 2016; Tahir et al., 2011; Zhang et al., 2014). Both models were tested following two steps. In the first step, the calibration and validation of both models was carried out under the control/reference period of over ten (10) (April 2000–March 2010) and two (2) hydrological years (April 2010–March 2012), respectively. The reasoning behind selecting this span for the calibration period (10 years) was to optimise the appropriate parameters for dry and wet years equally and then utilize their average values to simulate the scenario periods. To optimise the parameters by considering uncertainty issues, the Monte Carlo method based generalized likelihood uncertainty estimation (GLUE) approach was adopted to analyse uncertainties. Therefore, we run both models 100 times to get different sets of the parameters. HEC-HMS was applied by creating an optimisation trail setup and uncertainty simulations, implemented in the latest HEC-HMS version 4.2.1. For SRM, the initial parametric values were computed by adopting relationships and methods using observed and remotely sensed data (Martinec et al., 2008), and final calibration using trial and error, as suggested by Tahir et al. (2011) and Zhang et al. (2014). The evaluation of models parametric, uncertainty, the predictive uncertainty interval at 95% was estimated using GLUE approach. In the GLUE process, the number of model runs (100 in this case) was carried out with a large number of sets of parametric values. The achievement of accurate calibration was considered on the basis of two indices of P- and R-factors. The P-factor indicates the percent of observations bracketed by the 95% and the R-factor shows the relative band width. The goodness-of-fit for the calibration and prediction uncertainties were considered on the basis of the higher P-factor values from 0 to 100% and possible smallest R-factor (Shrestha et al., 2017). A detailed description of the GLUE process and uncertainty analysis is provided by Lehbab-Boukezzi et al. (2016) and Xue et al. (2018). In the second step, both models were utilized to simulate and compare the potential impact of climatic variations on streamflows for three distinct projected GCM-simulated scenarios. Moreover, performance of both hydrological models was examined on an annual and seasonal basis (winter or snow accumulation period, pre-monsoon or snowmelt period and monsoon season or extreme rainfall period) by using two well-known statistical indices, the Nash–Sutcliffe model efficiency coefficient (NSE) and the difference in volume (Dv%).

A. HEC-HMS Model Setup

The HEC-HMS is a standard rainfall-runoff model, developed by the United States Army Corps of Engineers for the simulation of rainfall-runoff of dendritic watershed systems (Scharffenberg and Fleming, 2006). The algorithm and parameters of HEC-HMS have been discussed in detail by several researchers (Azmat et al., 2016; Halwatura and Najim, 2013; Scharffenberg and Fleming, 2006). In this study, we applied the latest released HEC-HMS 4.2.1 version on a semi-distributed basis by dividing the Jhelum River basin into 22 sub-catchments (Fig. S6), on the basis of tributaries and data points available within the Jhelum River basin. Moreover, the distribution of sub-basins provides flexibility to users to define appropriate parametric values for each sub-basin by considering their individual characteristics (e.g. snow and glaciers, climate pattern, land use land cover, slope, soil type etc.). The HEC-HMS comprises of two major modules, i.e. the basin and meteorological modules. The basin module is used to incorporate the basin, i.e. catchment area, slope and reach length etc., and offers flexibility to choose an appropriate method to incorporate transfer, loss, channel routing and base flow while the meteorological module is used to select the evapotranspiration and snowmelt method. In the basin module, soil moisture accounting (SMA) (loss method), SCS unit hydrograph (transfer method), lag time (channel routing) and monthly average (base flow method) were selected to compute overland flows. The Penman-Monteith and temperature index methods were adopted for evapotranspiration and snowmelt simulations, respectively. The combination of different available methods in HEC-HMS for computation of streamflow components (i.e. loss, transfer, routing, base flow, evapotranspiration and snowmelt) was devised on the basis of a careful suitability analysis for the study region, as suggested by Azmat et al. (2017b). Moreover, the initial parametric values were extracted by using ASTER based global digital elevation model (GDEM), FAO (Food and Agriculture Organization) world soil maps data and Landsat 8 images for the land use land cover (LULC) classification (Figs. S7 and S8). On the other hand, for the transfer and channel routing, lag times (hrs) are required to define for sub-basins and reaches, which were estimated by employing the Soil Conversation Services (SCS) log equation. The values of degree-day-factor (DDF) in mm/°C/day, temperature lapse rate in °C/100 m, *px*-temperature, base temperature, are required to be defined in the snow module. The snowmelt contribution is strongly influenced by the DDF, therefore, different DDF (mm/°C-day) values for snow and ice were needed to be defined for each sub-basin. The lapse rate was computed by using observed and WFDEI temperature data available at different stations. The sub-basins were further divided into several elevation bands to distribute temperature variations over the sub-basin. The elevation bands help to process orographic distribution of temperature over the sub-basin for snowmelt using temperature lapse rate and observed air temperature. The number of elevation bands defines appropriate computation of temperature data for the sub-basins (Scharffenberg and Fleming, 2006). Further, the *px*-temperature is used to discriminate the form of rainfall occurrence (solid or liquid), while, the base temperature is responsible to define snowmelt. The source of initial values, range of final optimised parameters during the calibration processes (observed and GCMs-simulated climate data) are provided in Table S7.

B. Snowmelt Runoff Model (SRM) Setup

The SRM model, developed by Martinec et al. (2008) has been discussed in detail and applied by several researchers in different high-altitude catchments located in high Asia mountains (Azmat et al., 2016; Zhang et al., 2014). The daily zone-wise (ZW) streamflow simulations were carried out in a selected study basin which was divided into five altitude zones with a difference of 1000 m (at Mangla and Azad Pattan station) and with 500 m (at Garhi Habibullah, Muzaffarabad and Domel station) between two zones as suggested by Tahir et al. (2011). The ZW and season-wise (winter to summer) model parameters were optimised during control period (Table S8). The initial values of some parameters were extracted from previous studies (Tahir et al., 2011), while others (Table S9) were computed by using relationships given in SRM help manual. The different DDF (mm $°C^{-1}$ d^{-1}) values for snow (area less than 5000 m a.s.l.; 4 to 5.7) and ice (area above 5000 m a.s.l.; 5.7 to 7.4) were extracted from previous studies (Hock, 2003; Immerzeel et al., 2009). For each simulation (2000–2010 or 2030s, 2060s and 2090s) we used the corresponding temperatures for the computation of the respective lapse rate. Further, the ZW range of optimised parametric values and their description is given in Table S8.

5. Results and discussion

5.1. Evaluation of uncorrected GCM-simulations

CMIP5 GCM model evaluation and ranking was carried out by adopting the criteria defined in Section 4.2. Table 1, S4 and S5 depict the substantial biases between GCMs and current climate conditions to generate precipitation. Among eight GCMs, there were substantial

Table 1
(a) Biases (Pbias before corrections) between different statistical indices estimated for daily observed precipitation and GCM-simulations on annual and seasonal basis, during 1976–2005, for four best suitable GCMs. Pbias is the difference between observed and GCMs-simulations for each statistical index. In column 10, total of each identity (4 identities are dark gray, light gray, underlined and bold Italic) is given on which basis ranking is assigned in column 11. In column 11, the bold values show rank of the GCM by considering score values, (b) Ranking and evaluation of GCM-simulated basin-wide T_{max} (T_{min}), before bias corrections.

(a)

(1)	(2)	(3)	(4)	(5)	(6)	(7)	(8)	(9)	(10)	(11)
CMIP5 Models	**Statistics \Seasons**	**Mean (mm/day)**	**SD (mm/day)**	**Percentile (95%)**	**5-day max rainfall (mm)**	**%Wet days**	**Max dry spell length**	**Max wet spell length**	**Total of each identity**	**Overall Ranking**
BCC-CSM1.1	Annual	−0.16	−0.15	−0.39	4.1	0.02	−17	***−4***	8	**1**
	Winter	0.74	−0.24	−0.3	−15.2	0.1	−21	−9	6	
	Pre-monsoon	0.04	***−0.4***	−0.73	3.1	***0.06***	***−11***	***−7***	4	
	Monsoon	0.02	***0.45***	0.66	−10.5	0.17	−12	−5	***6***	
CMCC-CMS	Annual	***0.21***	−0.81	−3.2	34.6	***−0.07***	−12	2	6	**4**
	Winter	***0.75***	***−1.12***	−1.15	***−16.3***	0	−5	−3	4	
	Pre-monsoon	0.25	−0.35	−2.35	−9.5	−0.01	−9	−3	7	
	Monsoon	***−0.66***	0.33	−2.22	***19.4***	0.18	−5	2	***7***	
INMCM4	Annual	−0.12	−0.58	−0.15	7.5	−0.06	−14	−3	7	**2**
	Winter	0.4	−0.1	0.47	−14.05	0.09	−7	***−4***	10	
	Pre-monsoon	0.22	−0.19	0.23	−16.91	0.03	−5	−5	7	
	Monsoon	−0.47	−0.11	3.06	15.82	***0.2***	−6	***−3***	***3***	
IPSL-CM5A-LR	Annual	−0.34	***−0.83***	−1.76	−10.85	−0.03	***−20***	−4	7	**3**
	Winter	0.6	−0.53	***1.18***	−10.32	0.12	−12	−1	5	
	Pre-monsoon	***0.28***	0.15	***−0.84***	−26.39	0.08	−10	−4	4	
	Monsoon	−0.37	−0.16	1.05	7.46	0.15	−3	1	***5***	

(b) ***Observed data Obs_ μ (°C) = 24.81 (8.21); Obs_SD (°C) = 8.54 (7.43)***

Biases in Temperature, T_{max} (T_{min}) (°C)

CMIP5 models	**E_μ (°C)**	**E_SD (°C)**	**RMSE (°C)**	***R***	**Ranking**
BNU-ESM	−4.69 (-3.58)	2.42 (2.87)	8.12 (7.51)	0.78 (0.77)	5
BCC-CSM1.1	−2.31 (−2.57)	1.12 (1.09)	5.13 (5.27)	0.87 (0.81)	**1**
CMCC-CMS	***−3.11 (−2.68)***	1.61 (1.68)	***6.31 (6.84)***	***0.83 (0.81)***	**4**
CSIRO-MK3.6.0	−4.59 (−3.36)	2.59 (3.12)	8.92 (7.92)	0.81 (0.79)	6
ACCESS1.3	−4.37 (−4.14)	2.15 (3.15)	7.69 (9.34)	0.82 (0.79)	7
INMCM4	−1.59 (−2.09)	1.18 (1.27)	5.22 (5.42)	0.86 (0.85)	**2**
IPSL-CM5A-LR	−2.02 (−2.42)	***1.66 (1.89)***	5.53 (5.98)	0.84 (0.84)	**3**
CanESM2	−2.69 (−2.98)	2.36 (3.24)	8.51 (9.67)	0.81 (0.79)	8

Note: Negative (−) values shows overestimation and positive (+) values shows underestimation. Each identifier has rank according to biasness (e.g. dark, light Gray, underlines and bold Italic ranked 1, 2, 3 and 4, respectively, with respected to observed data). Detailed results of 8 GCMs are given in Table S4, S5 and Fig. S5.

differences between observed and GCM-simulations during the monsoon (July–Sep) and winter (Oct–March) periods, and some GCMs (i.e. BNU-ESM, BCC-CSM1.1) performed better during the monsoon season than in winter, and vice versa. Based on biases, Table 1 depicts BCC-CSM1.1, INMCM4, IPSL-CM5A-LR and CMCC-CMS which were ranked 1, 2, 3 and 4, respectively, on the basis of quantified statistical indices followed by observed climate variables. From the top ranked selected GCMs, each performed well with different indices i.e. BCC-CSM1.1 (ranked 1) and INMCM4 (ranked 2) performed well with the daily mean precipitation (mm/d), SD (mm/d), percentile (95%) and 5-days max rainfall (mm), while, IPSL-CM5A-LR (at 3) performed mixed with all indices and CMCC-CMS (at 4) performed well with maximum dry- and wet-spell length. Results depicted that most of the GCMs overestimated the mean precipitation (mm/d) during summer and SD (mm/d) and percentile (95%) during all seasons. Regarding 5-day maximum rainfall (mm), most overestimations were found during the winter and pre-monsoon seasons (Table 1a). In the case of maximum dry and wet spell lengths, almost all GCMs overestimated in comparison with the observed values in all seasons. In the case of temperature, Table 1b depicts the performance of GCM-simulations in comparison with observed temperature. According to statistics, there is a substantial difference between observed and GCMs-simulated temperature variables. The errors in mean (E_μ) values [with highest −4.69 (−3.58)] showed substantial overestimations, while, standard deviations (E_SD) values [with highest 2.59 (3.24)] showed slightly better efficiency with underestimations. The least RMSE and correlation coefficient values for T_{max} (T_{min}) were found to be 5.13 (5.27) and 0.78 (0.77), respectively. Overall, all the GCM-simulations of temperature showed better agreement with the observed data, however BCC-CSM1.1, INMCM4, IPSL-CM5A-LR and CMCC-CMS showed the best fit. The obtained results are corroborated by Lutz et al. (2016b), who conducted an investigation to scrutinize numerous GCMs for the UIB using an advanced envelop based climate model selection approach and suggested a better performance of GCMs (CSM1.1, INMCM4, IPSL-CM5A and CMCC-CMS) for both precipitation and temperature.

Table 2
Ranking of bias correction approaches employed for the correction of GCM-simulations of precipitation and T_{max} and T_{min}. Basin-wide statistical descriptors show performance of each bias correction approach.

Ranking of bias correction approaches		
Precipitation	T_{max}	T_{min}
1. Distribution mapping: RMSE = 2.01 (mm/d), MAE = 0.39 (mm/d)	1. Distribution mapping: RMSE = 2.03 (°C), MAE = 0.17 (°C)	1. Distribution mapping: RMSE = 2.09 (°C), MAE = 0.19 (°C)
2. Local intensity scaling (LOCI): RMSE = 2.89 (mm/d), MAE = 0.49 (mm/d)	2. Linear scaling: RMSE = 3.36 (°C), MAE = 0.29 (°C)	2. Linear scaling: RMSE = 3.39 (°C), MAE = 0.31 (°C)
3. Raw GCMs data: RMSE = 3.18 (mm/d), MAE = 0.63 (mm/d)	3. Raw GCMs data: RMSE = 5.58 (°C), MAE = 0.84 (°C)	3. Raw GCMs data: RMSE = 5.61 (°C), MAE = 0.89 (°C)

RMSE = Root mean square error; MAE = Mean absolute error.

5.2. Evaluation of bias correction approaches

Post-correction indices values showed that the raw GCM-simulations could be improved significantly (Table 2, S6 and Fig. S5). Fig. S5 depicts the responses of both bias correction approaches (LOCI and DM) to cope with uncertainties existed in raw GCM-simulations. The DM approach performed fairly well for percentile (95%), 5-days maximum rainfall (mm), maximum dry- and wet-spell length than LOCI. The LOCI showed considerable range of variability and still have biases of comparatively less magnitude than uncorrected but was classified as unfit to use for further analysis. The major biases could not be accommodated by the LOCI method existed in maximum dry- and wet-spell length (Fig. S5). Moreover, in the case of temperature (T_{min} and T_{max}) variables, both approaches significantly improved raw GCM-simulations. However, distribution mapping performed fairly well in terms of RMSE (°C) and MAE (°C) with 2.03 and 0.17 (for T_{max}) and 2.09 and 0.19 (°C) (for T_{min}), respectively, in comparison with linear scaling with 3.36 and 0.29 (for T_{max}) and 3.39 and 0.31 (°C) (for T_{min}), respectively (Table 2). In addition, the factual values of RMSE, correlation coefficient (R), and highest E_μ (°C) and E_SD (°C) given in Table S6 confirm the aforementioned statement. Holistically, Table 2 depicts that the LOCI (for precipitation only) and linear scaling (for temperature variables only) were able to partially remove the biases from GCM-simulations but remained unable to bring values closer to observed values. While the distribution mapping managed to bring model values closer to observations, the remaining biases may be associated with the influence of large spatial climate variability over the Jhelum River basin such as the monsoon and westerlies circulation precipitation patterns (Fig. S5). Overall, the distribution mapping approach provides best fits of both precipitation and temperature variables as confirmed by Teutschbein and Seibert (2010) and (2012).

5.3. Climate projections

5.3.1. Precipitation projections

Table 3a depicts annual and seasonal basin-wide (using Thiessen Polygon method) projected changes [absolute (percent)] in precipitation over Jhelum River basin. It is clear from the obtained results that maximum basin-wide precipitation increase was found during the monsoon period with 137.1 (7.33), 165.3 (10.49) and 183.2 mm (12.74%) for the 2030s, 2060s and 2090s, respectively, under RCP4.5-simulations. The winter season is ranked second with a projected increase by 85.39 (4.74%), 105.1 (10.09%) and 139.3 mm (15.14%) during the 2030s, 2060s and 2090s, respectively. It was noticed that the percentage of increase is similar at most instances, however, absolute values make a significant difference and show a better picture of climate projections. A slight decrease in precipitation was observed under RCP8.5-simualtions in comparison with RCP4.5-simulations. Fig. 3 depicts the potential change in precipitation and mean temperature using four GCMs. The maximum and minimum precipitation (mm) rise was observed for CMCC-CMS and IPSL-CM4A, respectively, on annual and seasonal basis under RCP4.5 and RCP8.5 scenarios. Overall, precipitation rise for CMCC-CMS was found significant in comparison with INMCM4, BCC-CSM1.1 and IPSL-CM4A. In Jhelum River basin, the investigation of spatial distribution of precipitation change is tremendously important due to the strong influence of contrasting climate patterns at different stations, as discussed in Section 2. Figs. S10 and S11 show an increase (annually) in projected precipitation with maxima at stations mainly influenced by monsoon pattern (i.e. Anantnag, Pulwama, Kotli, Gharidopata, Mangla, Kotli and Baramula) during scenario-periods for RCP4.5 and RCP8.5. The least projected increase (%) in precipitation is expected during the pre-monsoon season. Overall, RCP8.5 is following very similar spatial change patterns to RCP4.5. The maximum projected increase in precipitation was found at the stations influenced by monsoon precipitation pattern during monsoon, while, stations influenced by westerlies circulation pattern influenced most during winter. Interestingly, few stations (i.e. Narran, Srinagar and Burzil) are kind of hybrid stations with highly influenced by westerlies circulation and slightly by the monsoon season, however, the least increase in precipitation was observed during the winter season for all scenario-periods. Similarly, Murree, Gharidopata, Gujjar Khan, Balakot and Muzaffarabad are strongly influenced by monsoon precipitation patterns, however, precipitation percentage increase during the monsoon period was found to be very low. The precipitation projections suggest that the stations influenced by strong monsoon pattern can possibly be attributed to the monsoon intensity rise which is consistently found in climate model projections and scenarios. Overall, results indicate that the large spatial precipitation heterogeneity is likely to increase in Jhelum River basin under all scenarios and future periods.

5.3.2. Temperature projections

Fig. 3b depicts, in most instances, maximum basin-wide rise in temperature was noticed for CMCC-CMS and INMCM4 in comparison with BCC-CSM1.1 and IPSL-CM4A during annual and seasons, however, a significant rise was found during winter and pre-monsoon season. Although, a potential rise in temperature is expected during future periods of the 2030s, 2060s and 2090s for both RCPs, however, a temperature rise for RCP8.5 is expected to be more significant than for RCP4.5. Table 3b shows highest and extensive rise in T_{max} and T_{min} during the pre-monsoon season of the scenario-periods for RCP4.5 and RCP8.5. Similarly, the second highest rise in T_{max} and T_{min} was noticed during the winter season.

Additionally, Figs. S12 and S13 show spatial distribution of temperature change and explain the maximum increase in mean annual temperature at Gujjar khan, Planderi, Rawlakot, Kotli and Balakot stations by the 2030s for RCP4.5-simulations. An increase in temperature [1.3–2.77 (2030s), 2.2–3.71 (2060s) and 2.9–4.8 °C (2090s)] during winter is alarming for the hydrological system of this region with

Table 3
(a) Basin-wide (Thiessen Polygon method) projected changes in total precipitation, mm (%) and, (b) projected change in mean T_{max} (T_{min}), on annual and seasonal basis (winter, pre-monsoon and monsoon) under future scenarios of RCP4.5- and RCP8.5-simualtions, during 2030s (2011–2040), 2060s (2041–2070) and 2090s (2071–2100) in comparison with baseline period (1976–2005), over Jhelum River basin.

Season/period	RCP4.5			RCP8.5		
	2030s	2060s	2090s	2030s	2060s	2090s
(a) Basin-wide seasonal change in precipitation, mm (%)						
Annual (J-D)	69 (5.43)	118 (9.29)	155 (11.19)	64 (5.31)	112 (9.26)	150 (11.12)
Winter (O-M)	85.39 (4.74)	105.1 (10.09)	139.3 (15.14)	81.41 (4.66)	101.5 (10.01)	134.6 (14.98)
Pre-monsoon (A-J)	61.39 (6.29)	74.14 (8.7)	99.51 (11.48)	58.78 (6.27)	71.66 (8.66)	96.41 (11.39)
Monsoon (J-S)	137.1 (7.33)	165.3 (10.49)	183.2 (12.74)	132.1 (7.31)	157.6 (10.47)	177.3 (12.69)
(b) Basin-wide seasonal change (°C) in temperature T_{max} (T_{min})						
Annual (J-D)	1.76 (1.75)	2.42 (2.49)	3.49 (3.63)	1.86 (1.97)	3.33 (3.31)	4.62 (4.48)
Winter (O-M)	1.80 (1.81)	2.44 (2.61)	3.64 (3.74)	2.08 (2.13)	3.41 (3.37)	4.8 (4.58)
Pre-monsoon (A-J)	1.85 (1.86)	2.78 (2.62)	3.54 (3.59)	1.95 (1.97)	3.26 (3.16)	4.77 (4.42)
Monsoon (J-S)	1.59 (1.54)	2.27 (2.14)	3.14 (3.44)	1.57 (1.76)	3.12 (3.32)	4.23 (4.34)

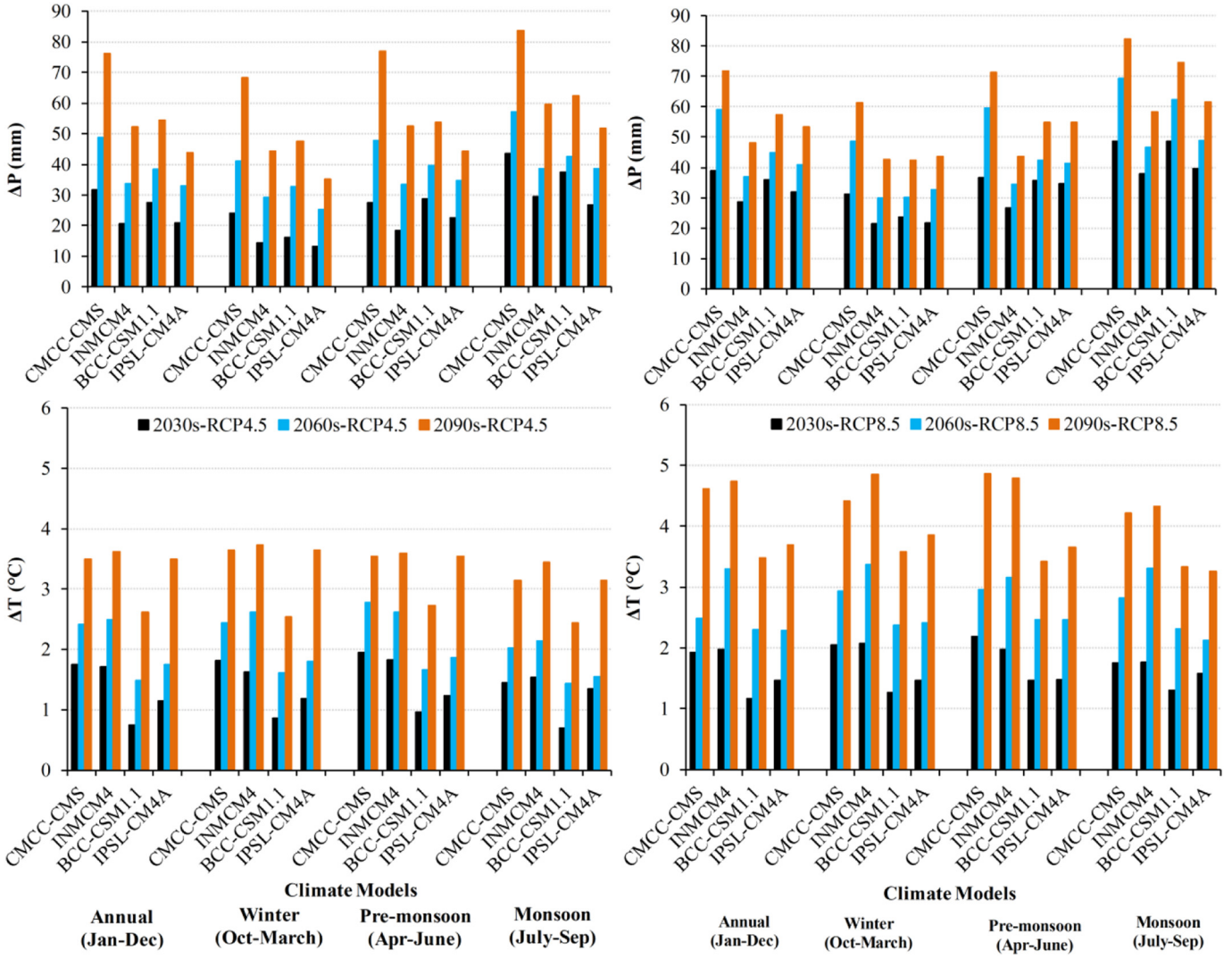

Fig. 3. Basin-wide mean annual and seasonal changes in precipitation (upper) and temperature (lower) under four different GCM-simulations for RCP4.5 and RCP8.5 scenarios.

important implications for snow accumulation and then melting during the pre-monsoon and monsoon seasons. A large increase in temperature which could eventually reduce the occurrence of rainfall in solid form during winter and consequently initiate the shrinkage of snow and glacier cover area in the basin leading to a reduction in summer discharge at the time of peak demand. Additionally, temperature increases during the pre-monsoon could also lead to early or rapid snowmelt runoff generation particularly from high-altitude zones of the basin, resulting in shrinkage of glacier area and early occurrence of spring-summer peak discharge. RCP8.5-simulations indicate an even stronger rise in mean temperature on annual and seasonal basis than the RCP4.5-simulations, with related more pronounced consequences for the cryosphere and the hydrology. Specifically, it was noticed that the stations at high-altitude are least affected with temperature rise (e.g. Narran, Burzil, Anantnag and Pulwama) in comparison with low-altitude under both RCP4.5- and RCP8.5-simulations (Figs. S12 and S13). Overall, the rise in precipitation over the study basin are slightly different from that explained by Lutz et al. (2016a) who reported the approximate ranges of rise in precipitation (5–12%) and temperature (3–4.5 °C) over different parts of the UIB at the end of 21st century under RCP4.5. For RCP8.5, slightly decreasing precipitation (−5 to −10%) and increasing temperature (4–6.5 °C) are expected between 2051 and 2100. In another study, Lutz et al. (2016b) reported that the range of rise in temperature (2.1–8.0 °C) over the UIB is substantial in comparison with the global average (1.8–4.4 °C) between 2071 and 2100. The slight discrepancy in outcomes using RCP8.5 may be attributed to the use of different GCM ensembles, projection (bias correction) approaches and hypothesis used in previous studies, such as Lutz et al. (2016a) and (2016b) used a delta approach for bias correction and provide ensemble results of GCMs. Similarly, Forsythe et al. (2014) used RCMs and reported a rise in annual precipitation and temperature over UIB by 18% and 4.8 °C, respectively, with an increase in precipitation intensity during the winter months under between 2071 and 2100 than 1961–1990, which is in-line with results obtained in the current study.

5.4. Application of hydrological models

Streamflow simulations were carried out at Muzaffarabad, Domel, Garhi Habibullah, Azad Pattan and Mangla dam stations by using HEC-HMS and SRM on annual and seasonal basis [winter (snow accumulation), snowmelt period (pre-monsoon) and extreme rainfall period (monsoon)]. The optimised results for uncertainty predictive band at 95% showed that both models performed fairly well with an acceptable range of predictive uncertainty band [(P-factor: 0.59–0.75, R-factor: 0.70–0.84 for HEC-HMS)] and [(P-factor: 0.62–0.77, R-factor: 0.74–0.89 for SRM)] at most instance (Fig. S9). Figs. 4 and 5 depict that both models simulated daily streamflows fairly well at all gauging stations during annual and seasonal analyses. The efficiency of both models was influenced by different factors such as seasons (e.g.

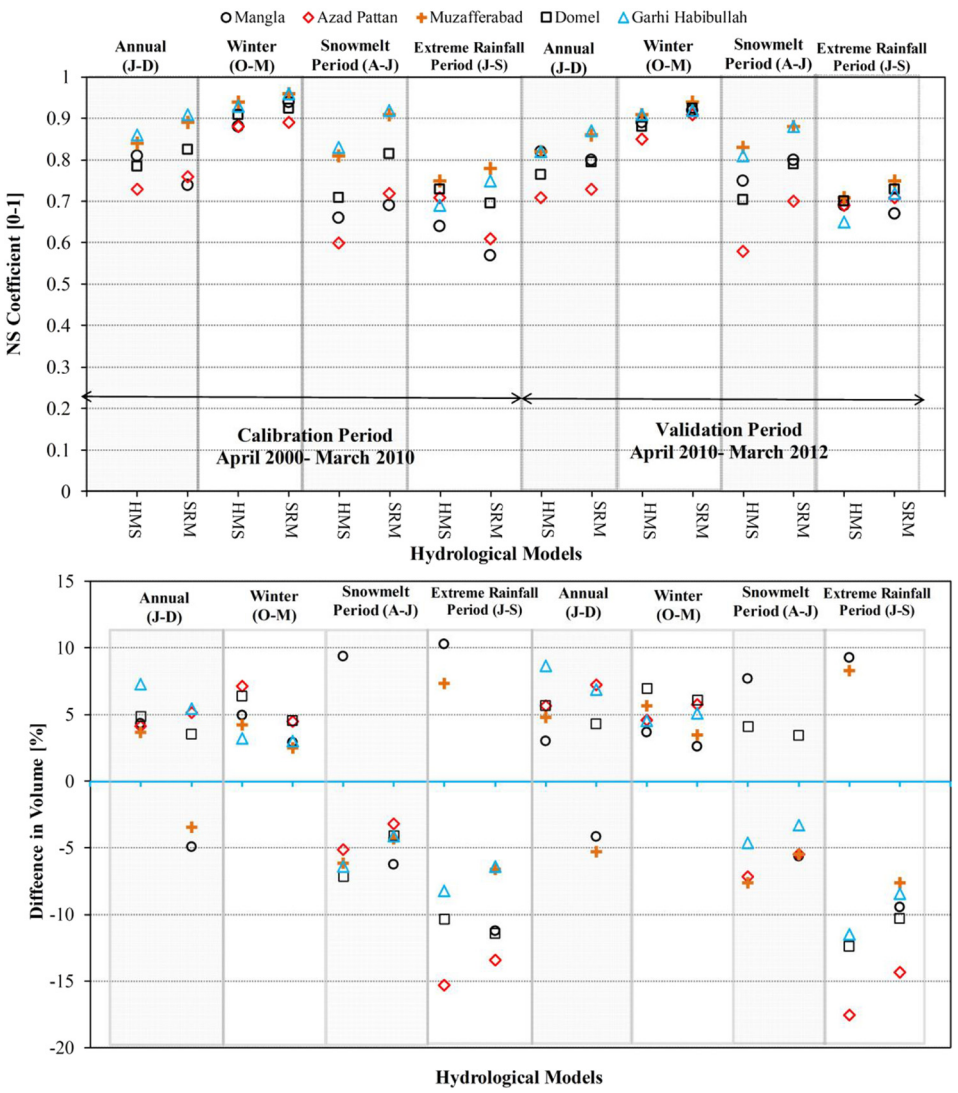

Fig. 4. Statistical comparison of streamflow simulations for HEC-HMS and SRM at five gauging stations (Mangla, Azad Pattan, Muzaffarabad, Domel and Garhi Habibullah) by using NS coefficient (upper) and percent (%) difference in volume (lower).

snowmelt or extreme rainfall period), catchment size and major runoff source (snowmelt- or rainfall-runoff). It was noticed that at all stations except Mangla, the HEC-HMS performed slightly less efficient in comparison with SRM with NSE values (annual basis) at Muzaffarabad (0.84 and 0.89), Domel (0.78 and 0.82), Garhi Habibullah (0.86 and 0.91) and Azad Pattan (0.73 and 0.76), for HEC-HMS and SRM, respectively. Additionally, during the snowmelt period (pre-monsoon), SRM performed significantly better than HEC-HMS at all gauging stations with NSE values of 0.91 and 0.81 (Muzaffarabad), 0.81 and 0.71 (Domel), 0.92 and 0.83 (Garhi Habibullah), 0.72 and 0.60 (Azad Pattan) and 0.69 and 0.66 (Mangla), respectively (Figs. 4 and 5). This efficiency may possibly be attributed to the major contribution of snowmelt due to an increase in the relative SCA of individual basins (Table S1). Interestingly, the HEC-HMS performed better than SRM during extreme rainfall periods (monsoon) for the stations mainly dominated by rainfall-runoff and monsoon precipitation pattern with NSE values for HEC-HMS and SRM of 0.73 and 0.69 (Domel), 0.71 and 0.61 (Azad Pattan) and 0.64 and 0.57 (Mangla Station), respectively. Conversely, at gauging stations which receive a major portion of water from snowmelt and are influenced by westerlies, SRM performed better than HEC-HMS with NSE values of 0.78 and 0.75 (Muzaffarabad), 0.75 and 0.69 (Garhi Habibullah), respectively. The aforementioned results suggest that the difference in efficiency of both models is based on the hydro-climatic, and seasonally dependent characteristics of the basins in relation with design structures and algorithms of the model. The SRM is a snowmelt runoff model and is designed to reproduce runoff generated by snow- and glacier-melt efficiently with integration of temperature and SCA. HEC-HMS is a rainfall-runoff model and can simulate rainfall generated runoff with accuracy (Azmat et al., 2016; Tahir et al., 2011). The sub-basins of Jhelum River are characterized by rainfall- and snow- or glacier-melt-runoff, and therefore, the better efficiency of SRM specifically at Muzaffarabad and Garhi Habibullah stations even during extreme rainfall period may be attributed to the dominance of snowmelt accumulation due to westerlies circulation, thereby, melt occurs during the pre-monsoon (snowmelt period). Similarly, HEC-HMS performed well during extreme rainfall period at Azad Pattan and Domel stations which may be attributed to the strong influence of monsoon precipitation pattern where maximum streamflows during extreme rainfall period are in liquid form. Overall, in seasonal simulations, models performed less efficiently as compared to the annual with exception of winter (NSE 0.78 for HEC-HMS and 0.93 for SRM) with NSE values 0.65 and 0.63 (HEC-HMS) and 0.68 and 0.55 (SRM) during snowmelt and extreme rainfall period, respectively. This may be associated with the absence of substantial streamflow during winter and shows both models are capable of reproduce base flow fairly well, as confirmed in literature (Azmat et al., 2016; Tahir et al., 2011). Additionally, at most instances,

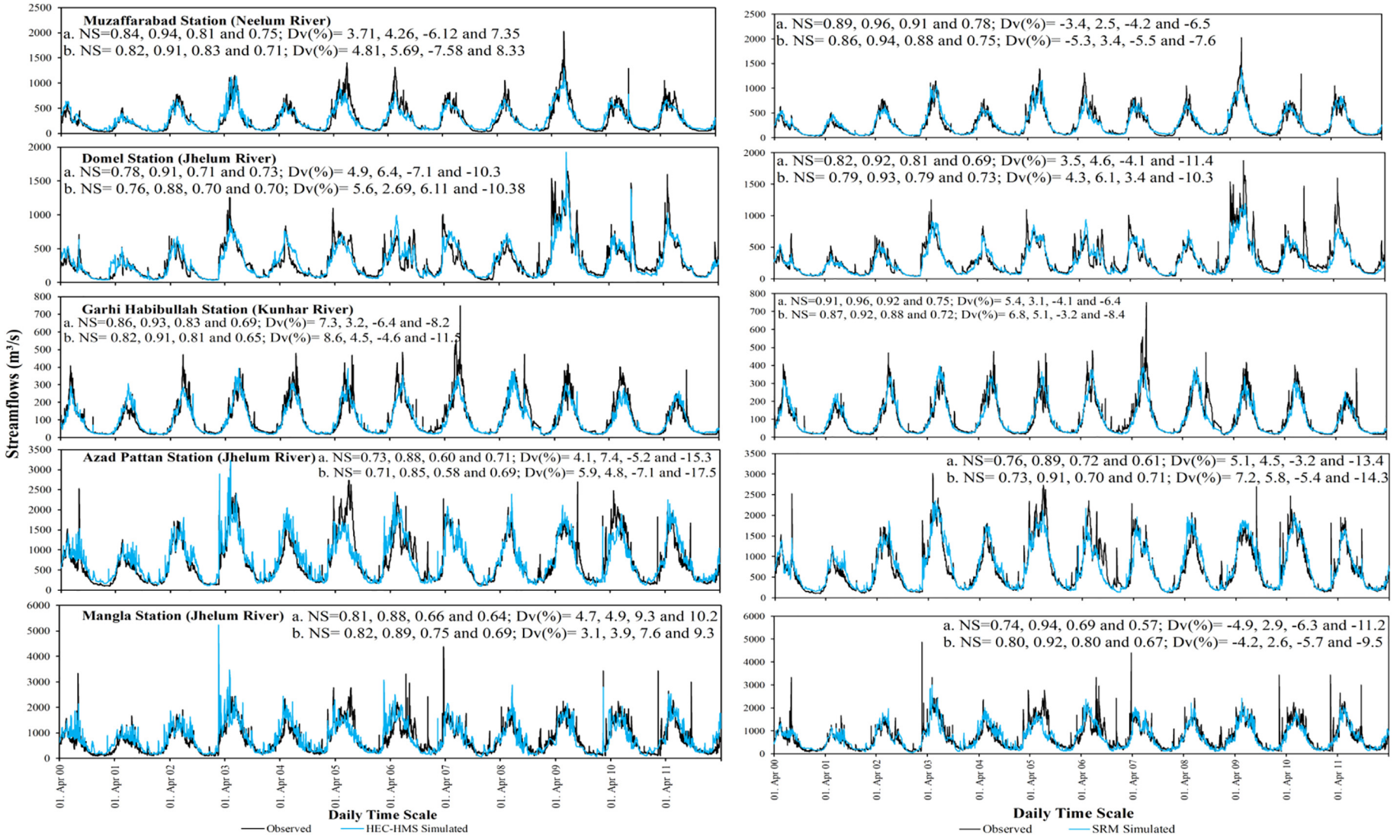
Muzaffarabad Station (Neelum River)
a. NS=0.84, 0.94, 0.81 and 0.75; Dv(%)= 3.71, 4.26, -6.12 and 7.35
b. NS= 0.82, 0.91, 0.83 and 0.71; Dv(%)= 4.81, 5.69, -7.58 and 8.33
Domel Station (Jhelum River)
a. NS=0.78, 0.91, 0.71 and 0.73; Dv(%)= 4.9, 6.4, -7.1 and -10.3
b. NS= 0.76, 0.88, 0.70 and 0.70; Dv(%)= 5.6, 2.69, 6.11 and -10.38
Garhi Habibullah Station (Kunhar River)
a. NS=0.86, 0.93, 0.83 and 0.69; Dv(%)= 7.3, 3.2, -6.4 and -8.2
b. NS= 0.82, 0.91, 0.81 and 0.65; Dv(%)= 8.6, 4.5, -4.6 and -11.5
Azad Pattan Station (Jhelum River)
a. NS=0.73, 0.88, 0.60 and 0.71; Dv(%)= 4.1, 7.4, -5.2 and -15.3
b. NS= 0.71, 0.85, 0.58 and 0.69; Dv(%)= 5.9, 4.8, -7.1 and -17.5
Mangla Station (Jhelum River)
a. NS=0.81, 0.88, 0.66 and 0.64; Dv(%)= 4.7, 4.9, 9.3 and 10.2
b. NS= 0.82, 0.89, 0.75 and 0.69; Dv(%)= 3.1, 3.9, 7.6 and 9.3
Streamflows (m³/s)
01. Apr 00
01. Apr 01
01. Apr 02
01. Apr 03
01. Apr 04
01. Apr 05
01. Apr 06
01. Apr 07
01. Apr 08
01. Apr 09
01. Apr 10
01. Apr 11
Daily Time Scale
Observed
HEC-HMS Simulated
a. NS=0.89, 0.96, 0.91 and 0.78; Dv(%)= -3.4, 2.5, -4.2 and -6.5
b. NS= 0.86, 0.94, 0.88 and 0.75; Dv(%)= -5.3, 3.4, -5.5 and -7.6
a. NS=0.82, 0.92, 0.81 and 0.69; Dv(%)= 3.5, 4.6, -4.1 and -11.4
b. NS= 0.79, 0.93, 0.79 and 0.73; Dv(%)= 4.3, 6.1, 3.4 and -10.3
a. NS=0.91, 0.96, 0.92 and 0.75; Dv(%)= 5.4, 3.1, -4.1 and -6.4
b. NS= 0.87, 0.92, 0.88 and 0.72; Dv(%)= 6.8, 5.1, -3.2 and -8.4
a. NS=0.76, 0.89, 0.72 and 0.61; Dv(%)= 5.1, 4.5, -3.2 and -13.4
b. NS= 0.73, 0.91, 0.70 and 0.71; Dv(%)= 7.2, 5.8, -5.4 and -14.3
a. NS=0.74, 0.94, 0.69 and 0.57; Dv(%)= -4.9, 2.9, -6.3 and -11.2
b. NS= 0.80, 0.92, 0.80 and 0.67; Dv(%)= -4.2, 2.6, -5.7 and -9.5
Daily Time Scale
Observed
SRM Simulated

Fig. 5. Comparison between observed and simulated streamflows of SRM (a) and, HEC-HMS (b), using observed climate data during calibration (April 2000 to March 2010) and validation period (April 2010 to March 2012) along with values of statistical descriptors at five streamflow measuring stations installed at different streams of the Jhelum River. In figures *a.* shows descriptor values during calibration period according to pattern of annual, winter, pre-monsoon and monsoon season and *b.* shows values during validation period.

SRM underestimates with negative Dv(% values), while HEC-HMS overestimates overall volume with positive values (Fig. 4). This may be associated with fact that the SRM is primarily designed for snow- and glacier-melt simulation, while HEC-HMS is a rainfall-runoff model.

In addition, Fig. 5 confirms the aforementioned statements and depicted that HEC-HMS can reproduce rainfall-generated-runoff peaks with higher accuracy than SRM, particularly during the winter and extreme rainfall period (monsoon). However, in most instances, it also produced some non-existing peaks or overestimated flood peaks reflected by Dv(%) values in Fig. 4. Although, several rapid flood peaks were poorly captured by SRM, it captured gradual variability in streamflow due to low intensity rainfall and snow- and glacier-melt, more efficiently than HEC-HMS. This may be associated with the sensitivity of the model's algorithm to specific climate variable (precipitation/temperature). The HEC-HMS model is highly sensitive to precipitation (Azmat et al., 2016), while SRM is less sensitive to precipitation and more to the temperature and SCA data (Tahir et al., 2011). The obtained SRM efficiency is similar to Zhang et al. (2014) in Buha Basin (Tibetan Plateau) with NS 0.73. While, slightly less than obtained by Tahir et al. (2011) in Hunza Basin (Central Karakoram) with NS 0.92, this is most likely due to large snow (80% during winter) and glacier (33%) cover in Hunza River. The obtained HEC-HMS results are similar to Meenu et al. (2013) and Kabiri et al. (2015) carried out in Tunga–Bhadra river basin, India and Klang River basin, Malaysia, respectively.

5.5. Hydrological predictions to changing climate

5.5.1. Impact of climate change on hydrological components

The contribution of different hydrological components in the overall hydrological cycle to a changing climate of the river basin is of high importance. This study is an attempt to simulate changes in major hydrological components for future scenario-periods, over a high-altitude snow-fed Jhelum River basin (Table 4 and Figs. 6, 7). SRM did not provide hydrological components separately, therefore, we used only HEC-HMS to simulate the changes for four components (i.e. rainfall-runoff, snowmelt-runoff, evapotranspiration and soil water storage) and two for SRM (i.e. rainfall-runoff, snowmelt-runoff), under the scenario-periods (Table 4). The simulated streamflows for the scenario-periods were compared with reference/control period, however, the observed data of evapotranspiration, rainfall-runoff, snowmelt-runoff, soil water storage were not available. Therefore, it is justifiable to compare the aforementioned components with simulated values during the control period (2000–2010), as suggested by Bajracharya et al. (2018).

When examining changes in soil water storage (SW) to changes in climate over the Jhelum River basin, during the scenario-periods on annual (mm) and seasonal (%) basis (Table 4 and Fig. 6), it is evident that the sub-basins located in high-altitude parts of the basin are less sensitive to soil water storage changes during the scenario-periods. This may possibly be attributed to the soil profile of the sub-basins, mainly consisting of bed rock and steep slope with low infiltration and storage capacity. The low-altitude parts of the basin are expected to change more in soil water storage due to extensive agriculture and tillage activities which allows irrigation water and precipitation to infiltrate. Moreover, parts of the basin located along the river reach are also expected to see substantial changes. This may be associated with flat topography and forest area which allows water to infiltrate in soil profile. Furthermore, on a seasonal basis, rises in precipitation and temperature might lead to maximum increase in soil water change in the soil profile. The increase in soil water storage during the pre-monsoon season might be due to complete melt of SCA and decline in soil saturation level throughout the Jhelum River basin. Overall, basin-wide change in soil water storage increases by 85 mm (6.3%), 92 mm (15%) and 98 mm (22.5%) during the 2030s, 2060s and 2090s, respectively, for RCP4.5 simulated by using HEC-HMS (Table 4).

It is apparent that evapotranspiration is expected to increase across the Jhelum River basin with availability of large soil water storage and rise in temperature during scenario-periods. Table 4 depicts a continuous increase in evapotranspiration (ET) during the 2030s, 2060s and 2090s with values of 288 (7.5), 304 (13.4) and 321 mm (19.8%), respectively, for RCP4.5 while a significant ET increase is expected for RCP8.5 during the scenario-periods. Similarly, on a seasonal basis, ET is substantially higher during the monsoon season in comparison with the pre-monsoon season and during the winter season. The spatial distribution of ET shows significant increases in ET across low-altitude sub-basins particularly dominated with agriculture activities. Despite rises in temperature and precipitation the high-altitude sub-basins are classified with low increase in ET percentage. This may be due to fact that high-altitude sub-basins are dominated by snow cover during the winter and pre-monsoon resulting in less intensive to ET increase. The ET during the monsoon is expected to increase substantially in comparison with the pre-monsoon during all scenario-periods under RCP4.5 and RCP8.5 (Fig. 6). This is most likely due to the availability of maximum soil water storage and significant rise in temperature during monsoon.

Precipitation, snow-fall and snow-melt are of critical importance for the annual hydrological cycle over high-altitude basins and temperature is a major driving factor. The change in temperature and precipitation over high-altitude basins alter SCA, snow depth, accumulation, melt-timings and melt-intensity. Fig. 7 depicts the low-attitude parts influenced by the monsoon pattern are more intended to rise in precipitation-runoff than the high-altitude. Additionally, in relation with precipitation rise, the monsoon precipitation-runoff is significantly increasing for the 2090s in comparison with the 2030s and 2060s. Notably, the response of precipitation-runoff during the pre-monsoon and winter season is significantly increasing most likely due to significant rise in temperature for the scenario-periods, as explained in Section 5.3. Further, Fig. 7 depicts the low-altitude sub-basins intended with very slight changes in snowmelt as compared to high-altitudes. Furthermore, on a seasonal basis, the pre-monsoon season is expected to receive significantly higher snowmelt-runoff from high-altitude

Table 4
Summary of basin-wide hydrological components simulated using HEC-HMS and SRM under projected scenarios of RCP4.5- and RCP8.5-simulations in comparison with control/reference period, over Jhelum River basin at Mangla dam station.

Scenarios/time periods		Totals of hydrological components, absolute values in mm (% increase)						
		Total P mm	HEC-HMS				SRM	
			Q Rain (mm)	Q Snowmelt (mm)	ET (mm)	SW (mm)	Q Rain (mm)	Q Snowmelt (mm)
Reference		1277	353	472.5	268	80	301	519
RCP 4.5	2030s	1346 (5.4)	385 (9.06)	520 (10.1)	288 (7.5)	85 (6.3)	329 (1.8)	544 (15.1)
	2060s	1395 (9.2)	411 (16.4)	536 (13.4)	304 (13.4)	92 (15)	351 (8.6)	569 (20.4)
	2090s	1432 (12.2)	435 (23.8)	527 (11.5)	321 (19.8)	98 (22.5)	373 (15.4)	591 (25.9)
RCP 8.5	2030s	1371 (7.4)	388 (9.9)	534 (13.1)	297 (10.8)	86 (7.5)	336 (4.10)	556 (17.6)
	2060s	1428 (11.8)	413 (16.9)	527 (11.5)	318 (18.7)	94 (17.5)	363 (12.3)	578 (22.3)
	2090s	1467 (14.9)	438 (24.1)	522 (10.4)	342 (27.6)	101 (26.2)	384 (18.8)	598 (26.7)

Note: Given values of ET and soil water storage (SW) was estimated by using HEC-HMS.

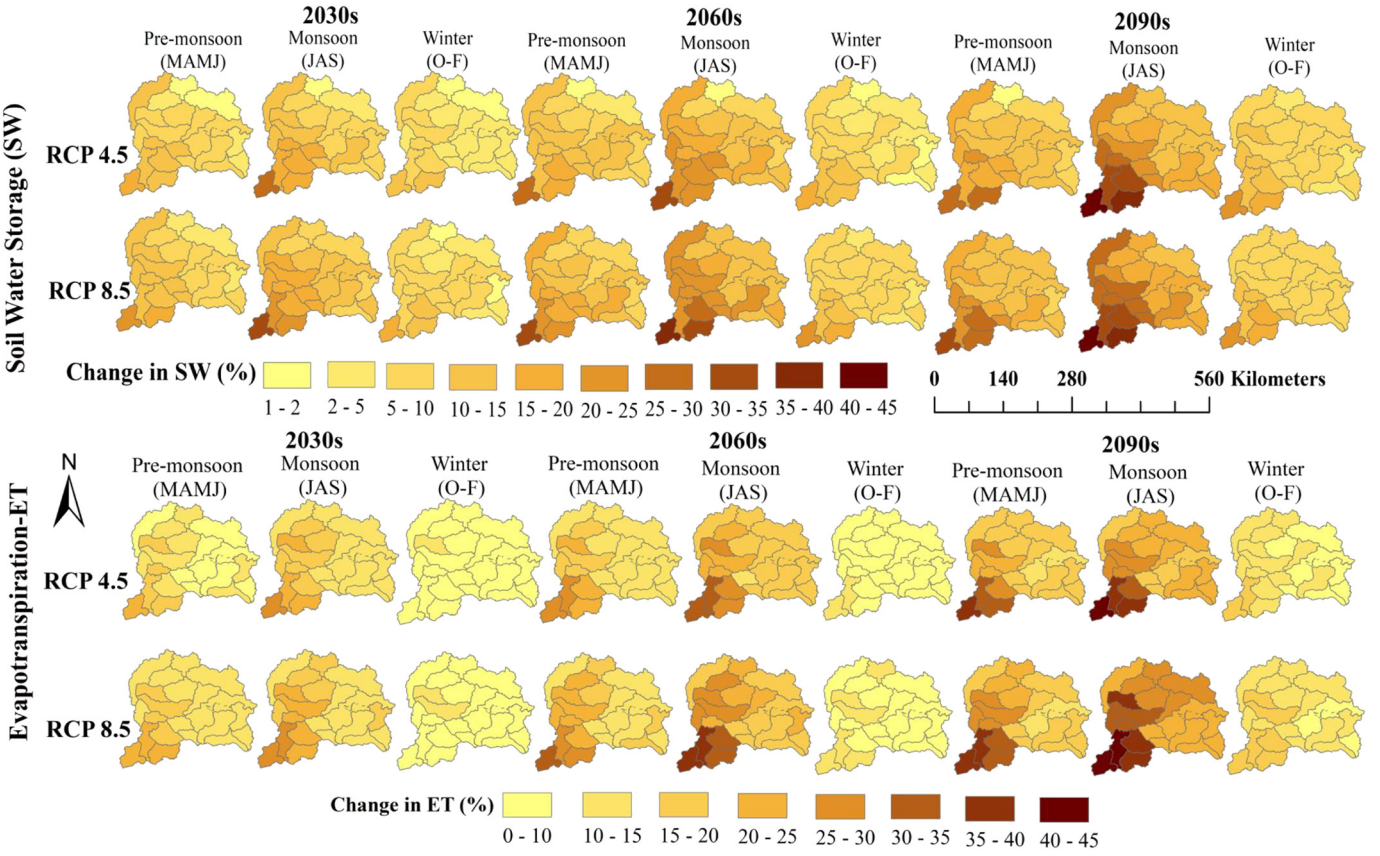

Fig. 6. Spatial and seasonal change in soil water storage (SW) (upper) and evapotranspiration (ET) (lower) for RCP4.5 and RCP8.5 ensembles during 2030s, 2060s and 2090s, relative to reference period (2000–2012), using HEC-HMS hydrological model.

sub-basins in comparison with the monsoon period. Notably, for RCP4.5, annual basin-wide snowmelt-runoff contribution during the 2060s (536 mm (%)) is higher than for the 2030s (520 mm (10.1%)) and 2090s (527 mm (11.5%)), for HEC-HMS (Table 4). A continuous decrease of annual snowmelt-runoff is observed for RCP8.5 using HEC-HMS [(534 mm (13.1%), 527 mm (11.5%) and 522 mm (10.4%))] during the 2030s, 2060s and 2090s, respectively. Conversely, a continuous substantial increase in rainfall-runoff [385 mm (9.06%), 411 mm (16.4%) and 435 mm (23.8%)] contribution is most likely due to a substantial rise in monsoon precipitation, using HEC-HMS. Furthermore, for SRM, the snowmelt along with rainfall-runoff is continuously increasing under the scenarios-periods (Table 4 and Fig. 7). Similar results are observed during the pre-monsoon season (Fig. 6). Further, the monsoon contribution during the 2030s is higher than in the 2060s and 2090s, particularly for high-altitude areas of the basin. Broadly, snowmelt patterns for RCP4.5 and RCP8.5 are similar, however, RCP8.5 produces slightly higher snowmelt than RCP4.5 particularly during pre-monsoon of the 2030s. Furthermore, the winter snowmelt is slightly increasing, while pre-monsoon and monsoon snowmelt is decreasing for the scenario-periods. This is most likely related to two reasons; first, during the 2030s, the increase in snow accumulation during winter due to a rise in precipitation particularly over high-altitude sub-basins is influenced by the westerlies. Secondly, the winter snowmelt increase during the 2060s and the 2090s is most likely due to the influence of temperature rise over low-altitude sub-basins where during the control period precipitation occurs in solid form but melts within few days or will occur in liquid form under the scenario-periods. This temperature rise could alter the snowline of the Jhelum River basin under the scenario-periods. The results presented in this study are in-line with Lutz et al. (2016a) and (2014), who used GCMs to estimate rainfall-, snowmelt- and glacier-melt-runoff over multiple catchments located in high mountain Asia and reported an increase of approximately 8% (RCP4.5) and 17% (RCP8.5) liquid precipitation contribution with increase or consistent trends for snowmelt-runoff contribution between 2071 and 2100 over UIB.

5.5.2. Streamflows to changing climate

The climate change impacts on streamflow of the Jhelum River basin using HEC-HMS and SRM was examined by considering 2000–2010 as a reference period. Table 5 indicates an increase in streamflow on annual and seasonal basis during scenario-periods for four GCMs (INMCM4, BCC-CSM1.1, IPSL-CM5A-LR and CMCC-CMS) under RCP4.5- and RCP8.5. The maximum increment was found for CMCC-CMS in comparison with INMCM4, BCC-CSM1.1 and IPSL-CM5A-LR. In most instances, maximum streamflow during pre-monsoon periods was increased between 2030s and 2060s, in comparison between the 2060s and 2090s, particularly for GCMs which showed a stronger rise in temperature (e.g. CMCC-CMS and INMCM4). For example, using CMCC-CMS-simulations under RCP4.5, the projected HEC-HMS-simulations were increased more than double from 116 m^3/s (7.9%) to 365 m^3/s (24.9%) from 2030s to 2060s, respectively, in comparison with the 2090s (387 m^3/s (26.5%)). Similar peculiar hydrological behaviour can be noticed during snowmelt period for HEC-HMS-simulations using CMCC-CMS and INMCM4 model projections for the 2060s and 2090s. For the monthly streamflows in April in the 2090s, HEC-HMS produced more streamflow in comparison with the 2060s, and conversely, the streamflow during May, 2090s, were found significantly smaller than 2060s, for INMCM4- and CMCC-CMS-simulations under both RCPs (Fig. 8a and b). These results suggest a shift of the hydrological regime (from May to April) due to temperature rise and early snowmelt. The significant rise in temperature under CMCC-CMS- and INMCM4-simulations may be responsible to expedite early snowmelt which maximizes pre-monsoon streamflow through snow and glacier-melt April 2060s and 2090s.

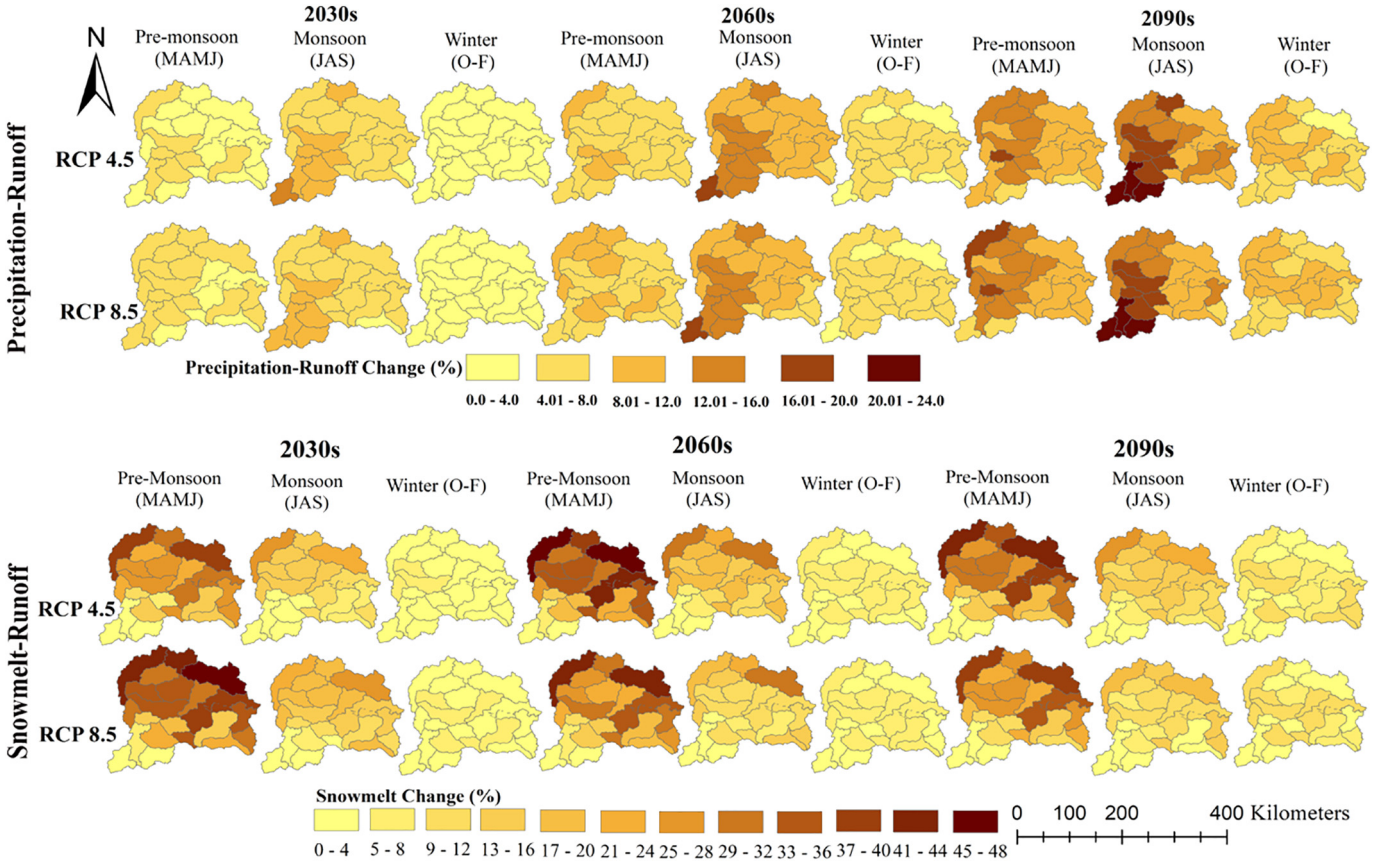

Fig. 7. Spatial and seasonal change in precipitation-runoff (upper) and snowmelt-runoff (lower) for RCP4.5 and RCP8.5 ensembles during 2030s, 2060s and 2090s, relative to reference period (2000–2012), using HEC-HMS hydrological model.

On the other hand, during extreme rainfall periods, the produced streamflows are not as high as during the snowmelt period. Interestingly, in most instances, it was observed that during the monsoon season (extreme rainfall period) the HEC-HMS generated streamflows almost doubled [104 m^3/s (9.4%), 185 m^3/s (20.8%) and 250 m^3/s (28.1%)] as compared to SRM [49 m^3/s (5.5%), 109 m^3/s (12.3%) and 180 m^3/s (20.2%)] during the 2030s, 2060s and 2090s, respectively, under CMCC-CMS-RCP4.5. Conversely, during pre-monsoon periods, results for CMCC-CMS-RCP4.5-simulations for SRM [174 m^3/s (12%), 397 m^3/s (27.1%) and 510 m^3/s (34.9%)] generated significant higher streamflows as compared to HEC-HMS [116 m^3/s (7.9%), 315 m^3/s (21.2%) and 387 m^3/s (26.5%)] during the 2030s, 2060s and 2090s, respectively. The aforementioned statement is also confirmed by GCMs-ensemble results with increases in HEC-HMS simulated streamflow [261 m^3/s (18.5%) and 363 m^3/s (24.8%)] as compared to SRM [311 m^3/s (21.1%) and 421 m^3/s (28.8%)] which showed significant increasing contributions during the 2060s and 2090s, for RCP4.5-ensembles (Table 5). Additionally, mean factorial seasonal values clearly defined the peak of Jhelum River flows dominated by the snow- and glacier-melt during pre-monsoon season (April–June) of 2000–2010 (1462 m^3/s) and 2030s, 2060s and 2090s [(1553 m^3/s, 1827 m^3/s and 1849 m^3/s for HEC-HMS) and (1636 m^3/s, 1859 m^3/s and 1972 m^3/s for SRM)], for RCP4.5 ensembles. A 1 °C rise in temperature will result in a pre-monsoon mean streamflow increase of 70 m^3/s (5.1%), 89.9 m^3/s (6.1%) and 69.2 m^3/s (4.7%) for HEC-HMS, and 75.1 m^3/s (5.13%), 101.8 m^3/s (6.7%) and 94.1 m^3/s (6.43%) for SRM, during the 2030s, 2060s and 2090s, respectively, under RCP8.5. This difference was more prominent for SRM simulations in comparison with HEC-HMS under all GCM-simulations under RCP8.5 which might be due to the greater rise in temperature for RCP8.5 than RCP4.5.

There are regional hydro-climate reasons behind the changes in hydrological behaviour of the study basin. The aforementioned statement is further confirmed by the local climate characteristics such as the monsoon season which mainly influences this region during the end of June up to the start of September with a peak during July and August, in contrast to other adjoining river basins (e.g. Upper Indus basin) (Archer and Fowler, 2008). Westerlies dominate during February and March, which mainly hits the high-altitude parts of the region (e.g. Narran and Burzil). Fig. 8a and b depict that the HEC-HMS simulations during monsoon period are mainly contributed by precipitation under scenario-periods. SRM based estimates project significant increases in streamflow during the pre-monsoon or snowmelt periods, mainly contributed by a rise in temperature variables over the study basin (Fig. 8c and d). The temperature rise expedites snowmelt processes from the end of March to the end of May with streamflows (for SRM) ranging from 878 to 2119 m^3/s and 981 to 2209 m^3/s during the 2060s and 2090s, respectively, for CMCC-CMS-simulations under RCP4.5, which is almost twice as much as for the reference-period (589 to 1681 m^3/s). Additionally, the SRM simulated peaks declined abruptly during the monsoon period but still a considerable amount of water was produced by the model in comparison to reference-period. The rise in precipitation could also contribute in streamflow only during monsoon season in form of liquid. A rise in temperature and winter precipitation could influence streamflows in two ways; first, winter temperature even after the rise is still less than the critical or *px*-temperature resulting in snow accumulation and subsequent rise, involving snowmelt process during the early pre-monsoon season. Second, a significant rise in temperature could alter the hydrological regime of the river by shifting precipitation form (solid to liquid) at low-altitude zones of the basin and early snowmelt runoff generation

Table 5
Projected changes in streamflow on annual and seasonal basis (winter, pre-monsoon and monsoon) estimated by using HEC-HMS and SRM with projected climate data of RCP4.5- and RCP8.5-simulations for four (4) scrutinized GCMs, in comparison with control/reference period (2000–2010), over Jhelum River basin at Mangla dam station.

Change in streamflows at Mangla station in m^3/s (%)													
Scenarios		RCP4.5						RCP8.5					
GCMs		2030s		2060s		2090s		2030s		2060s		2090s	
	Seasons	HMS	SRM	HMS	SRM	HMS	SRM	HMS	SRM	HMS	SRM	HMS	SRM
INMCM4	Annual	61 (8.09)	59 (7.8)	170 (22.4)	122 (16.1)	196 (25.8)	179 (23.6)	98 (13)	71 (9.4)	212 (27.9)	137 (18.1)	255 (33.7)	198 (26.1)
	Winter	18 (5.4)	41 (12.1)	50 (14.6)	63 (18.4)	90 (26.3)	88 (25.7)	31 (9.01)	47 (13.8)	62 (18.2)	72 (21.3)	106 (31.2)	106 (31)
	Pre-monsoon	109 (7.5)	104 (7.1)	261 (18.5)	298 (20)	350 (24.1)	390 (26.7)	113 (7.7)	124 (8.5)	292 (20)	324 (22.1)	371 (24.9)	415 (28.4)
	Monsoon	99 (11.1)	51 (5.7)	185 (20.8)	94 (10.5)	223 (25.1)	150 (16.9)	130 (14.6)	65 (7.4)	231 (26)	110 (12.4)	338 (38)	165 (18.5)
BCC-CSM1.1	Annual	62 (8.2)	41 (5.5)	118 (15.5)	99 (13.1)	169 (22.2)	148 (19.5)	76 (10.1)	58 (7.6)	142 (18.7)	122 (16.1)	187 (24.7)	165 (21.8)
	Winter	19 (5.6)	10 (3.1)	44 (13)	33 (9.9)	62 (18.1)	48 (14)	27 (7.9)	20 (6)	53 (15.5)	48 (14)	71 (21)	62 (18.1)
	Pre-monsoon	104 (7.3)	91 (6.2)	228 (15.6)	230 (15.7)	331 (22.6)	359 (24.6)	112 (7.7)	111 (7.6)	229 (15.7)	271 (18.5)	314 (21.2)	387 (26.4)
	Monsoon	95 (10.7)	54 (6.1)	155 (17.4)	100 (11.3)	220 (24.7)	137 (15.4)	109 (12.2)	79 (8.8)	182 (20.5)	124 (13.9)	252 (28.3)	151 (17)
IPSL-CM5A-LR	Annual	47 (6.2)	47 (6.2)	114 (15)	110 (14.6)	163 (21.4)	165 (21.8)	63 (8.3)	65 (8.6)	125 (16.5)	138 (18.2)	189 (24.9)	192 (25.3)
	Winter	8 (2.6)	15 (4.5)	28 (8.4)	35 (10.2)	46 (13.5)	49 (14.5)	14 (4.2)	30 (8.9)	37 (10.9)	58 (17)	57 (16.8)	75 (22)
	Pre-monsoon	105 (7.3)	110 (7.5)	244 (16.7)	278 (19)	355 (24.2)	428 (29.2)	119 (8.1)	130 (8.9)	269 (18.4)	312 (21.3)	391 (26.7)	460 (31.5)
	Monsoon	64 (7.2)	47 (5.3)	153 (17.2)	95 (10.7)	204 (23)	135 (15.2)	103 (11.6)	70 (7.9)	158 (17.8)	124 (13.9)	249 (28)	158 (17.7)
CMCC-CMS	Annual	64 (8.3)	80 (10.6)	165 (21.8)	164 (21.6)	207 (27.3)	222 (29.2)	66 (8.7)	100 (13.2)	179 (23.6)	184 (24.2)	219 (28.9)	243 (32.1)
	Winter	22 (6.6)	49 (14.4)	55 (16.3)	74 (21.8)	95 (28)	99 (29)	27 (7.9)	53 (15.7)	61 (17.9)	81 (23.9)	100 (29.5)	105 (30.8)
	Pre-monsoon	116 (7.9)	174 (12)	315 (21.2)	397 (27.1)	387 (26.5)	510 (34.9)	118 (8.1)	194 (13.3)	396 (27.1)	412 (28.2)	427 (29.2)	536 (36.6)
	Monsoon	104 (9.4)	49 (5.5)	185 (20.8)	109 (12.3)	250 (28.1)	180 (20.2)	92 (10.4)	76 (8.7)	198 (22.2)	159 (17.9)	250 (28.1)	228 (25.6)
Ensemble	Annual	56 (7.4)	58 (7.5)	141 (18.6)	123 (16.3)	183 (24.1)	178 (23.5)	75 (10)	73 (9.7)	164 (21.6)	145 (19.1)	212 (28)	199 (26.3)
	Winter	16 (5.1)	28 (8.5)	44 (13)	51 (15)	73 (21.4)	71 (20.8)	24 (7.2)	37 (11.1)	53 (15.6)	64 (19)	83 (24.6)	87 (25.4)
	Pre-monsoon	105 (7.3)	119 (8.1)	261 (18.5)	311 (21.1)	363 (24.8)	421 (28.8)	131 (9.4)	139 (9.5)	293 (19.8)	332 (22)	330 (22.6)	449 (30.7)
	Monsoon	84 (9.5)	50 (5.6)	169 (19)	99 (11.2)	224 (25.2)	150 (16.9)	108 (12.2)	78 (8.8)	192 (21.6)	129 (14.5)	272 (30.6)	175 (19.7)

Note: Annual (Jan to Dec), Winter (Oct to March), Pre-monsoon (April to June) and Monsoon (July to Sep).

at high-altitude zones, as suggested by Yao et al. (2012) for Tibetan Plateau and surroundings. Although, in most instances, the peak of the hydrological regime is not altered (naturally in May), but early or immediate runoff response of snow- and glacier-melt due extensive rise in temperature for CMCC-CMS and INMCM4 tends to shift regime. This fact is clear from Fig. 8 which depicts the slight shift of regime from April to March under the projected scenarios. The substantial rise in temperature could cause a substantial decline in snow accumulation and thereby snowmelt-runoff contribution and overall shift of intra-annual Jhelum River flows, particularly, in April and May. These declines in flows could result in less liquid form precipitation during February and March, resulting in snow and glacier mass loss under future scenarios, as suggested by Lutz et al. (2016a) and Yao et al. (2012). The obtained results in this study are in-line with studies carried out by Lutz et al. (2014) and (2016a) who suggested substantial increases in temperature and precipitation over the Upper Indus Basin (UIB) which could alter the snow- and rainfall-runoff proportion across the seasons. Furthermore, the main streamflow increase is caused by snow- and glacier-melt due to a temperature rise with a combination of precipitation increases over different gauging stations in the UIB. Based on current and previous studies (Kraaijenbrink et al., 2017; Lutz et al., 2014) it can be concluded that due to the continuous increase in temperature and precipitation over the Himalayas, at the end of this century, temperature is going to be a more influential variable to affect snow, glaciers and precipitation for the hydrological cycle. It could therefore be necessary to alter practises related to the operation of reservoirs and irrigation downstream of the Mangla dam. The construction of large capacity reservoirs could prove important to managing the changes in seasonal water availability and overall quantity in view of water demand and flood protection issues.

6. Conclusions

This study examined the impact of climate change on climate variables and major hydrological components (evapotranspiration, soil water storage rainfall- and snowmelt-runoff,) by investigating GCMs, bias correction approaches and hydrological models over the snow- and glacier-fed high-altitude scarcely-gauged Jhelum River basin. The changes in streamflow were estimated by using the HEC-HMS and SRM models to simulate water availability in Jhelum River basin under different future scenario-periods. The conclusions drawn by analysing obtained results in this study are as follows:

The analysis and ranking of CMIP5 model runs proved BCC-CSM1.1, INMCM4, IPSL-CM5A-LR and CMCC-CMS to be the most suitable among eight GCMs in the high-altitude Jhelum River basin. Furthermore, all three bias correction approaches were able to improve basic statistical indices such as mean daily values. However, only DM was found capable to correct other statistical indices. Therefore, DM could be a better choice for bias correction, particularly over high-altitude snow- and

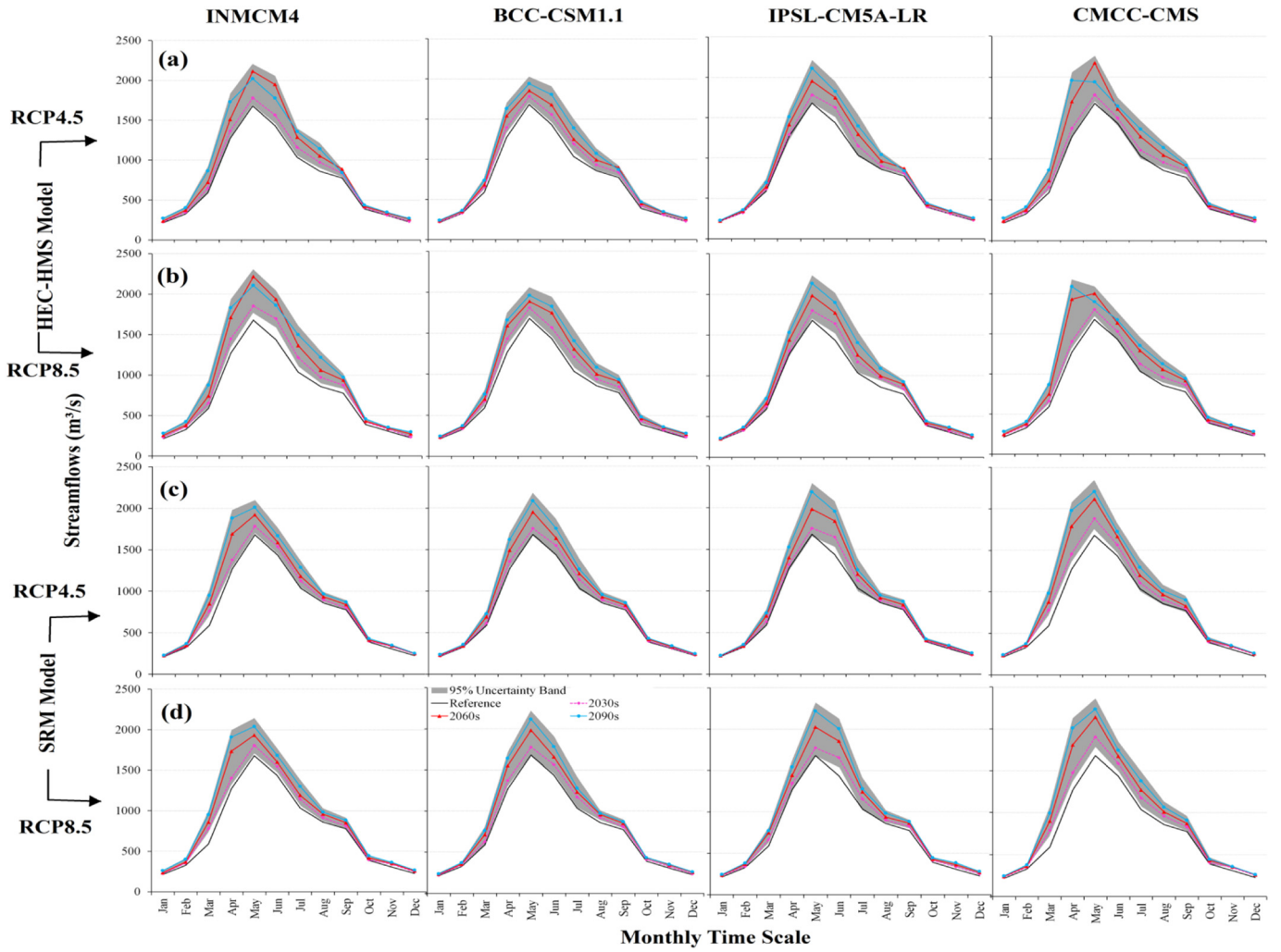

Fig. 8. Average annual hydrographs for four scrutinized GCMs (INMCM4, BCC-CSM1.1, IPSL-CM5A-LR and CMCC-CMS) projected scenario periods (2030s, 2060s and 2090s) of Jhelum River basin at Mangal dam. Row (a) and (b) shows the simulation of HEC-HMS model, row (c) and (d) shows simulation of snowmelt Runoff Model (SRM), using GCMs-simulated climate data for RCP4.5 and RCP8.5 model ensembles.

glacier-fed basins where uncertainty in GCM-simulations could be very high.

The WFDEI (gridded daily temperature and precipitation) data is a feasible option to cope with data limitation issues for hydrological investigations to changing climate in high-altitude, scarcely gauged catchments. The availability of WFDEI data at large temporal scale (1979–2012) is suitable for the bias correction of GCM-simulations and parameterisation of hydrological models.

The application of different hydrological models (HEC-HMS and SRM) with different algorithms and structures provides a clear picture of suitability over the Jhelum River basin or similar catchments. Results reveal that both models performed fairly well during the control period (reference) at five gauging stations installed across Jhelum River and provide good agreement between observed and predicted streamflows by using gauged and WFDEI precipitation and temperature data. SRM performed slightly better for streamflow simulations than HEC-HMS, particularly during pre-monsoon (snowmelt period) at the stations which receive dominant snowmelt contribution (i.e. Muzaffarabad, Garhi Habibullah, Azad Pattan and Domel). However, the HEC-HMS provides several other hydrological components (evapotranspiration, soil water storage, snowmelt- and rainfall-runoff) separate as output which helps to understand the hydrological behaviour of the catchments with different characteristics. Due to less sensitivity to precipitation data, SRM could be a better option for high-altitude scarcely-gauged catchments to reduce errors in the precipitation contribution to streamflow predictions.

Subsequently, the CMCC-CMS and INMCM4 models produced a maximum rise in annual temperature and precipitation over Jhelum River basin during the scenario-periods. The results of the projected scenario periods (2030s, 2060s and 2090s) showed a significant increase in basin-wide precipitation (69–155 mm for RCP4.5) and temperature range (1.86–4.62 °C for RCP8.5). Consequently, the evapotranspiration (27.6%), soil water storage (26.2%) and snowmelt-runoff (10.4%) and rainfall-runoff (24.1%) simulated using HEC-HMS, is expected to increase for RCP8.5 by the 2090s. Additionally, the average annual streamflows of the catchment are expected to increase by 75 m^3/s (10%), 164 m^3/s (21.6%) and 212 m^3/s (28%), for RCP8.5 using HEC-HMS and by 73 m^3/s (9.7%), 145 m^3/s (19.1%) and 199 m^3/s (26.3%) for RCP8.5 using SRM, during 2030s, 2060s and 2090s, respectively. Further, by the rise in climate variables, particularly, temperature could alter the state of the snow and glacier cover in the Jhelum River basin and could shift the hydrological regime of the river, resulting in snow and glacier mass loss. The projected streamflow is clearly dominated by snow- and glacier-melt most likely due to temperature rise during pre-monsoon period. This alteration in the basin hydrology could substantially impact the agricultural irrigation and cropping patterns,

domestic water use, hydroelectric power generation and ecosystems downstream of the Mangla dam. Water management of the basin should therefore start to consider future changes in river runoff.

Acknowledgement

The authors would like to acknowledge the financial support provided by the Swiss government under the "Swiss Government excellence Scholarship" program. This study was supported by the Higher Education Commission (HEC) of Pakistan under National Research Program for Universities (NRPU) with project # 6003. The Authors would like to thanks Benjamin Aubrey Robson from University of Bergen for English review.

Conflict of interests

The authors declare that they have no conflict of interest.

Appendix A. Supplementary data

Supplementary data to this article can be found online at https://doi.org/10.1016/j.scitotenv.2018.05.206.

References

Archer, D.R., Fowler, H.J., 2008. Using meteorological data to forecast seasonal runoff on the River Jhelum, Pakistan. J. Hydrol. 361, 10–23.
Azmat, M., Choi, M., Kim, T.-W., Liaqat, U.W., 2016. Hydrological modeling to simulate streamflow under changing climate in a scarcely gauged cryosphere catchment. Environ. Earth Sci. 75:1–16. https://doi.org/10.1007/s12665-015-5059-2.
Azmat, M., Liaqat, U.W., Qamar, M.U., Awan, U.K., 2017a. Impacts of changing climate and snow cover on the flow regime of Jhelum River, Western Himalayas. Reg. Environ. Chang.:1–13 https://doi.org/10.1007/s10113-016-1072-6.
Azmat, M., Qamar, M., Ahmed, S., Hussain, E., Umair, M., 2017b. TgL a Proceedings of the 1o" Orld Congress of EWRA TPanta Rhei", 5–9 July 2017, Athens, Greece.
Bajracharya, A.R., Bajracharya, S.R., Shrestha, A.B., Maharjan, S.B., 2018. Climate change impact assessment on the hydrological regime of the Kaligandaki Basin, Nepal. Sci. Total Environ. 625, 837–848.
Beniston, M., Stoffel, M., 2016. Rain-on-snow events, floods and climate change in the Alps: events may increase with warming up to 4 °C and decrease thereafter. Sci. Total Environ. 571, 228–236.
Bolch, T., et al., 2012. The state and fate of Himalayan glaciers. Science 336, 310–314.
Dahri, Z.H., Ludwig, F., Moors, E., Ahmad, B., Khan, A., Kabat, P., 2016. An appraisal of precipitation distribution in the high-altitude catchments of the Indus basin. Sci. Total Environ. 548, 289–306.
Forsythe, N., et al., 2014. Application of a stochastic weather generator to assess climate change impacts in a semi-arid climate: the Upper Indus Basin. J. Hydrol. 517, 1019–1034.
Halwatura, D., Najim, M., 2013. Application of the HEC-HMS model for runoff simulation in a tropical catchment. Environ. Model. Softw. 46, 155–162.
Hock, R., 2003. Temperature index melt modelling in mountain areas. J. Hydrol. 282, 104–115 (doi:Temperature index melt modelling in mountain areas).
Immerzeel, W.W., Droogers, P., De Jong, S., Bierkens, M., 2009. Large-scale monitoring of snow cover and runoff simulation in Himalayan river basins using remote sensing. Remote Sens. Environ. 113:40–49. https://doi.org/10.1016/j.rse.2008.08.010.
Jiang, Y., Liu, C., Li, X., Liu, L., Wang, H., 2015. Rainfall-runoff modeling, parameter estimation and sensitivity analysis in a semiarid catchment. Environ. Model. Softw. 67, 72–88.
Kabiri, R., Bai, V.R., Chan, A., 2015. Assessment of hydrologic impacts of climate change on the runoff trend in Klang Watershed, Malaysia. Environ. Earth Sci. 73:27–37. https://doi.org/10.1007/s12665-014-3392-5.
Kraaijenbrink, P., Bierkens, M., Lutz, A., Immerzeel, W., 2017. Impact of a global temperature rise of 1.5 degrees Celsius on Asia's glaciers. Nature 549, 257.
Lehbab-Boukezzi, Z., Boukezzi, L., Errih, M., 2016. Uncertainty analysis of HEC-HMS model using the GLUE method for flash flood forecasting of Mekerra watershed, Algeria. Arab. J. Geosci. 9, 751.
Liaqat, U.W., Choi, M., Awan, U.K., 2015. Spatio-temporal distribution of actual evapotranspiration in the Indus Basin irrigation system. Hydrol. Process. 29, 2613–2627.
Lutz, A., Immerzeel, W., Shrestha, A., Bierkens, M., 2014. Consistent increase in high Asia's runoff due to increasing glacier melt and precipitation. Nat. Clim. Chang. 4, 587–592.
Lutz, A.F., Immerzeel, W., Kraaijenbrink, P., Shrestha, A.B., Bierkens, M.F., 2016a. Climate change impacts on the upper Indus hydrology: sources, shifts and extremes. PLoS One 11, e0165630.
Lutz, A.F., ter Maat, H.W., Biemans, H., Shrestha, A.B., Wester, P., Immerzeel, W.W., 2016b. Selecting representative climate models for climate change impact studies: an advanced envelope-based selection approach. Int. J. Climatol. 36, 3988–4005.
Martinec, J., Rango, A., Roberts, R., 2008. SRM Snowmelt Runoff Model user's Manual. New Mexico State University, Las Cruces, New Mexico.
Meenu, R., Rehana, S., Mujumdar, P., 2013. Assessment of hydrologic impacts of climate change in Tunga–Bhadra river basin, India with HEC-HMS and SDSM. Hydrol. Process. 27:1572–1589. https://doi.org/10.1002/hyp.9220.
Rodell, M., et al., 2004. The global land data assimilation system. Bull. Am. Meteorol. Soc. 85, 381–394.
Scharffenberg, W.A., Fleming, M.J., 2006. Hydrologic Modeling System HEC-HMS: User's Manual. US Army Corps of Engineers, Hydrologic Engineering Center.
Shrestha, N.K., Du, X., Wang, J., 2017. Assessing climate change impacts on fresh water resources of the Athabasca River basin, Canada. Sci. Total Environ. 601, 425–440.
Tahir, A.A., Chevallier, P., Arnaud, Y., Neppel, L., Ahmad, B., 2011. Modeling snowmelt-runoff under climate scenarios in the Hunza River basin, Karakoram range, Northern Pakistan. J. Hydrol. 409:104–117. https://doi.org/10.1016/j.jhydrol.2011.08.035.
Taylor, K.E., Stouffer, R.J., Meehl, G.A., 2012. An overview of CMIP5 and the experiment design. Bull. Am. Meteorol. Soc. 93, 485–498.
Teutschbein, C., Seibert, J., 2010. Regional climate models for hydrological impact studies at the catchment scale: a review of recent modeling strategies. Geogr. Compass 4, 834–860.
Teutschbein, C., Seibert, J., 2012. Bias correction of regional climate model simulations for hydrological climate-change impact studies: review and evaluation of different methods. J. Hydrol. 456, 12–29.
Weedon, G.P., Balsamo, G., Bellouin, N., Gomes, S., Best, M.J., Viterbo, P., 2014. The WFDEI meteorological forcing data set: WATCH forcing data methodology applied to ERA-interim reanalysis data. Water Resour. Res. 50, 7505–7514.
Xue, L., Yang, F., Yang, C., Wei, G., Li, W., He, X., 2018. Hydrological simulation and uncertainty analysis using the improved TOPMODEL in the arid Manas River basin, China. Sci. Rep. 8, 452.
Yao, T., et al., 2012. Different glacier status with atmospheric circulations in Tibetan Plateau and surroundings. Nat. Clim. Chang. 2, 663.
Zhang, G., Xie, H., Yao, T., Li, H., Duan, S., 2014. Quantitative water resources assessment of Qinghai Lake basin using snowmelt runoff model (SRM). J. Hydrol. 519, 976–987.